Chapter 3

Disruption of regional primary structure of the Sierra Nevada batholith by the Kern Canyon fault system, California

Nadin, ES, and Saleeby, JB, Division of Geological and Planetary Sciences, California Institute of Technology, MC 100-23, Pasadena, CA 91125

Abstract

Regional spatial variation patterns in igneous emplacement pressures, initial $^{87}Sr/^{86}Sr$ (Sr_i), zircon U/Pb ages and pluton bulk compositions of the Sierra Nevada batholith (SNB) are disrupted by the ~130 km long Proto-Kern Canyon fault (PKCF), a Late Cretaceous ductile shear zone in the southern SNB. Vertical displacement and horizontal shortening across the PKCF in its early history are roughly constrained by the disruption of regional primary batholithic structure that is recorded in petrologic and geochemical spatial variation patterns. The disruption of these patterns suggests that the PKCF underwent 1) subvertical west-directed reverse faulting that was instrumental in the exhumation and deep exposure of the southern part of the SNB, and 2) southward-increasing reverse/thrust displacement. Disruption of otherwise smoothly varying geobarometric gradients across the central part of the PKCF suggests up to ~10±5 km of east side up reverse displacement across the shear zone. Southward from this area the PKCF truncates, at an oblique angle, the petrologically distinct axial zone of the SNB, which suggests that up to ~25 km of normal shortening occurred across the southern part of the PKCF. Normal shortening is further supported by the coincidence of the Sr_i = 0.706 isopleth with the PKCF from the point of initial truncation southward. Zircon U/Pb ages from plutons emplaced along the shear zone during its activity indicate that this shortening and vertical displacement commenced by 95 Ma and was abruptly overprinted by dominantly dextral displacement with small east side up reverse components by 90 Ma. Conventional structural and shear fabric analyses, in conjunction with geochronological data, indicate that at least ~15 km of dextral shear/slip occurred along

the zone between 90–86 Ma, and another 12±1 km of dextral slip occurred along the northern segment of the zone between 86–80 Ma. This later 12±1 km of dextral slip branched southwestward, abandoning the main trace of the shear zone near its central section, as the ductile-brittle Kern Canyon fault (KCF). Dextral shearing in the ductile regime was replaced by brittle overprinting by 80 Ma.

The timing of initiation and the duration of reverse-sense displacement along the PKCF correspond closely to the shallow flat subduction of the Franciscan-affinity Rand schist along the Rand fault beneath the southernmost SNB. In its southern reaches, the PKCF flattens into the Rand fault system, suggesting that it behaved like a lateral ramp. Post-90 Ma dextral shear along the PKCF is suggested to have partitioned at least part of the Farallon plate's tangential relative displacement component during an increase in subduction obliquity. Late-stage dextral ductile shear and early-phase brittle overprints on the PKCF–KCF system are coeval with tectonic denudation of the southernmost SNB. Geometric relations of the system's terminal ductile and early brittle history with orthogonal extensional structures pose the possibility that the southern segment of the PKCF, along with the younger KCF, behaved as a transfer system during the extensional phases of tectonic denudation of the southernmost SNB, leading to exposure of the oblique crustal section we see today.

Introduction

Understanding how large-volume magmatic arcs remain structurally coherent in the face of significantly varying subduction parameters, such as the dip and degree of obliquity of the subducting plate, is fundamental to understanding the structure and growth of continental crust. Arguably this is *the* question in the tectonics of the Cordilleran mountain belt of the western Americas. Variations in the magnitude of subduction obliquity commonly are manifest as the decoupling of normal and tangential fault displacements within arc–forearc domains (cf. Jarrard, 1986). Variations in the dip of the subducting plate influence cycles of subduction accretion and erosion, as well as intra-arc contractile versus extensional deformation (cf. Gutscher, 2001). The Sierra Nevada batholith (SNB) constitutes a critical segment of the North American Cordilleran batholithic belt, having formed in response to Cretaceous subduction of the Farallon plate beneath the California region. In Late Cretaceous time, the Farallon plate followed varying angles of subduction obliquity (Engebretson et al., 1985; Stock and Molnar, 1988; Kelley and Engebretson, 1994). A zone of intra-arc strike-slip faulting (Busby-Spera and Saleeby, 1990; Tikoff and Greene, 1994; Greene and Schweickert, 1995; Tobisch et al., 1995; Tikoff and Saint Blanquat, 1997) in the Sierra Nevada region, as well as inner trench wall strike-slip displacements in the Franciscan subduction complex (McLaughlin et al., 1988; Jayko and Blake, 1993), are suggested to have arisen from dextral-sense obliquity in the plate trajectory. Furthermore, the dip of the Farallon slab is suggested to have undergone significant variations during Late Cretaceous time (Dickinson and Snyder, 1978). In the southernmost Sierra Nevada region, these variations drove cycles of intra-arc shortening and extensional deformation (Malin et al., 1995; Wood and Saleeby, 1998; Saleeby, 2003). The net result of varying subduction-tangent and subduction-normal parameters is that the southern SNB is structurally more complex than the central and northern SNB. As a result, the southern SNB deviates from the well-preserved, intact primary geochemical and petrologic spatial variations of the central and northern SNB. This paper focuses on the relationship between intra-arc deformation and the disruption of these otherwise regionally coherent spatial variations in the southern SNB.

Large sets of isotopic data from batholithic complexes have been widely applied as a means to map at coarse scales the major tectonic features of continental basement (cf. Kistler and Peterman, 1978). Most noteworthy have been efforts to map fossil lithospheric structures in large-volume magmatic arcs (cf. Kistler, 1990), and efforts to document large displacements of batholithic rocks by superimposed structures (cf. Silver and Mattinson, 1986). Recently, the apparent attenuation of regional isotopic variation patterns along a major intra-batholithic shear zone was paired with structural data to approximate high-magnitude finite strain along the western Idaho batholith (Giorgis et al., 2005). Extensive investigations in the SNB have provided comprehensive data sets of geobarometry, initial $^{87}Sr/^{86}Sr$ (Sr_i), and U/Pb zircon ages (Kistler and Peterman, 1978; Saleeby and Sharp, 1980; Stern et al., 1981; Chen and Moore, 1982; Saleeby et al., 1987, 1990, 2007 and this volume; Ague and Brimhall, 1988, 1997; Chen and Tilton, 1991; Pickett and Saleeby, 1993; Brady et al., 2004; Coleman et al., 2004). In this paper, we synthesize these data and integrate them with geologic mapping and shear strain analysis to help constrain the kinematic history of the Proto-Kern Canyon fault (PKCF), a ~130 km long, intra-arc strike-slip fault that was instrumental in the disruption of the southern SNB. Conventional geologic mapping and shear strain analysis have placed reasonable constraints on dextral offset patterns along the system (Saleeby and Busby-Spera, 1986, 1993; Busby-Spera and Saleeby, 1990; Nadin, 2007; Saleeby and Nadin, in prep.). Vertical displacement and crustal shortening components have remained elusive, however, due to a lack of suitable markers. We recognize regionally continuous spatial variations in the geochemistry, petrology, wall rock stratigraphy, and depth of emplacement that characterize the entire Cretaceous SNB and extend into adjacent segments of the Cordilleran batholithic belt. The primary goal of this paper is to present data on the disruption of these regional patterns by the PKCF system, and to integrate these disruptions with structural data to offer a more complete kinematic analysis of the PKCF.

Geologic Background

The SNB is a composite batholith that formed largely between 130–80 Ma by sequential large-volume magma pulses into an accretionary orogenic complex that developed along the western edge of North America (Fig. 1). In Cretaceous time, the southern SNB continued southward in continuity with the southern California batholith (SCB), which was disrupted and is now dispersed as fault blocks of the Mojave Desert and the Salinia terrane of coastal central California. The southernmost SNB was tectonically partitioned from the SCB by the east-west striking, Neogene–Quaternary Garlock fault. It has been proposed that sinistral slip along the Garlock fault localized along a transverse inflection in the southernmost SNB crust that developed as a result of shallow slab subduction beneath the SCB in Late Cretaceous time (Saleeby, 2003). The mantle lithosphere was left intact beneath the greater SNB to the north, where subduction remained steeper (Ducea and Saleeby, 1998), and shallow slab subduction led to exposure of an oblique crustal section through the southernmost SNB across the inflection zone by southward increasing tectonic denudation. Primary structural integrity thus contrasts sharply between most of the SNB and its related SCB extension. The region and principal structures that we focus on are in the transition zone between these two differently preserved segments of the regional batholithic belt.

The study area lies along the oblique crustal section of the southernmost SNB, between latitudes 35˚ and 36.25˚ N and longitudes 118.25˚ and 118.5˚ W (Figs. 1 and 2). This region contains nearly 50 plutons, ranging in age from 105–84 Ma, and in composition from gabbro to granite. These plutons are grouped into five intrusive suites (Fig. 2). The suites include the regionally extensive 105-98 Ma Bear Valley and 95–84 Ma Domelands suites, which underlie the entire southwestern and eastern regions of the study area, respectively. The Domelands suite extends northward beyond the limits of the study area. A third regionally extensive suite (the 101–95 Ma Needles suite) intrudes out the northern end of the Bear Valley suite and extends for an unknown distance to the north of the study area. Less extensive are the 105–102 Ma Kern River and the 100-94 Ma South Fork suites.

Regional-scale petrologic spatial variation patterns that typify the SNB are expressed in the study area. In general the older plutons, and suites, lie in the western part of the batholith, and overall the plutons show a transition from intermediate (dioritic to tonalitic) to felsic (granodioritic to granitic) compositions from west to east. This west to east variation in bulk composition is mimicked by regional variations in Sr_i, with less radiogenic isotopic compositions to the west and more radiogenic compositions to the east (Saleeby et al., 1987; Kistler and Ross, 1990; Pickett and Saleeby, 1994). Pluton emplacement pressures within the SNB also vary from west to east, but there is a second trend in emplacement depths as well. The west to east trend is a decrease of ~2–3 kb (Ague and Brimhall, 1988); this typifies much of the SNB north of the study area. The second trend occurs in the study area and extends southward to the southern terminus of the range. It entails a southward increase of ~6–8 kb (Ague & Brimhall, 1988; Pickett & Saleeby, 1993; Dixon, 1995; Ague, 1997; Brady et al., 2004; and this study). The southern pressure gradient is also expressed in the contact metamorphic assemblages of pendant rocks, which were metamorphosed in albite-epidote to hornblende hornfels facies with significant domains of hornfelsic textures at the shallowest levels of the study area. At deeper levels in the batholith, the contact metamorphism of pendant rocks resulted in the development of high-strain tectonites in amphibolite facies, and, at deepest levels, local granulite facies with substantial zones of migmatization.

Shallow-level contact metamorphism resulting in hornfelsic textures developed adjacent to the Kern River intrusive suite and along the margins of related hypabyssal sills. Structural and stratigraphic relations of the Kern River suite are critical to the analyses in this paper because they provide an additional paleo-depth constraint. Plutons of this suite constitute epizonal levels beneath the coeval Erskine Canyon silicic volcanic sequence. The K1, K3 and K4 units of this suite (Fig. 2) are constrained by structural relations to have been emplaced at less than ~6 km depths (Saleeby et al., Fig. 3, this volume). The surface level conditions implicit in the volcanic stratigraphy of the Erskine Canyon sequence, and the shallow-level emplacement depths of the underlying plutons, provide a critical barometric equivalent datum for the 105–102 Ma time interval that may be used in conjunction with geobarometric data on neighboring plutons to decipher spatial variation patterns in depth of exposure.

The metamorphic country rocks of the southern SNB are composed primarily of metasedimentary and metavolcanic/hypabyssal assemblages. These wall rocks generally crop out as N–NNW striking, steeply dipping pendants stretched between plutons or between different zones of hosting plutons (Figs. 1 and 2). Some of the larger pendants contain resolvable sparsely fossiliferous stratigraphic sequences shown to be part of the lower Jurassic–Triassic Kings sequence (Saleeby and Busby-Spera, 1986; 1993), but many of the pendant rocks in the study area are metamorphosed and deformed to the extent that they may only be constrained by regional relations to be lower Paleozoic to Jurassic in age. These pre-batholithic country rocks constituted the local basement for the syn-batholithic Erskine Canyon volcanic sequence. As shown on Figure 2, a roughly N-S striking belt of pendants appears to have been instrumental in localizing ductile shear of the PKCF (Nadin and Saleeby, 2004; Nadin, 2007).

The Proto-Kern Canyon fault

Structural Setting

The PKCF extends from the southern end of the Sierra Nevada northward to latitude ~36.6° N (Figs. 1 and 2). This study focuses on the southern ~110 km of the shear zone, and in particular on the area between latitudes 35.5º N and 36.2º N. Included in our analysis is the Kern Canyon fault (KCF). The northern ~90 km of the KCF coincides with the northern segment of the PKCF, but at latitude ~36.75º N, the KCF branches southwestward out of the shear zone (Fig. 2). This branching point defines the split between the northern and southern segments of both the PKCF and the KCF. The KCF is a steeply dipping, narrow, partly ductile but mainly brittle structure that is shown below to have had up to ~12±1 km of Cretaceous dextral displacement. Although field studies and low-temperature thermochronological data indicate that much of the brittle faulting along the KCF represents late Neogene–Quaternary normal-sense remobilization (Nadin and Saleeby, 2001; Nadin, 2007; Maheo et al., in prep.), the ~12 km of earlier dextral slip are actually an integral part of the PKCF dextral slip history. Two additional shear/fault zones that branch out of the PKCF–KCF system are also critical to our analysis (Figs. 1 and 2). First, at latitude ~35.5˚ N the ~17 km long King Solomon Ridge shear zone branches northwest out of the southern segment of the PKCF, terminating against the KCF (Fig. 2). This shear zone shows strong early phase, coaxial, ductile fabrics with superposed apparent south side up normal(?) sense ductile-brittle shears (Saleeby and Nadin, in prep., Maheo et al., in prep.). Secondly, the ~40 km long dextral sense Farewell fault/shear zone branches northwest out of the northern PKCF at latitude ~36.2˚ N, and traverses the Mineral King pendant (Ross, 1986; Busby-Spera and Saleeby, 1987; du Bray and Dellinger, 1981). This vertical structure exhibits both ductile and brittle dextral shear fabrics that spread over an ~5 km width adjacent to the PKCF. Accordingly, ductile fabrics proximal to the branching point are not readily resolved as belonging to the PKCF or to the Farewell fault.

The main high-strain zones of the PKCF were localized along the edges of Late Cretaceous-aged plutons that were cooling through solidus conditions, and within adjacent steeply dipping metasedimentary pendant rocks (Busby-Spera and Saleeby, 1990; Nadin and Saleeby, 2004; Saleeby et al., this volume; Nadin, 2007). Along its northern segment, the PKCF is typically a 2–5 km wide zone of NNW striking, steeply east-dipping, pervasively schistose to phyllonitic pendant rocks and granitic mylonites with structural domains containing concordant brittle shear fabrics. Along the southern segment, ductile shear fabrics locally thin to as narrow as ~1 km and the eastward dip of the zone progressively shallows as it curves to the southwest and then to the southeast near its southern termination (Fig. 3). South of latitude ~35.3˚ N the thickness of the high-strain zone widens again to ~4 km. The southernmost ~5 km of the PKCF has been termed the eastern Tehachapi shear zone by Wood and Saleeby (1998) (Fig. 2). In this area, the shear zone merges with subhorizontal lower crustal tectonites that are pervasive near the base of the SNB plate that lies above the Rand fault system (Fig. 3). The Rand fault system is a regional low-angle ductile–brittle structure that places underplated accretionary prism assemblages of the Franciscan complex beneath the SCB as well as the southernmost SNB (Cheadle et al., 1986; Li et al., 1992; Malin et al., 1995; Yan et al., 2005).

Localization of the PKCF along the western margin of the youngest belt of plutons, which in the study area corresponds to the 95–84 Ma Domelands suite, led to development of granitic mylonites with S-C fabrics, asymmetric quartz ribbons, sigmoidal feldspar porphyroclasts, and mica fish. These are particularly well developed in the Goldledge and Cannell Creek granitic bodies (Fig. 2). Further south, the western margins of the more expansive Claraville pluton exhibits high-strain blastomylonitic to annealed gneissic textures that only locally display non-coaxial shear fabrics. Lineation orientations within both mylonitized granitic and pendant rocks throughout the length of the shear zone vary from subhorizontal to subvertical, with the steeply plunging sets typically overprinted by the shallowly plunging sets. Shallower plunging lineations show predominantly dextral motion, and in some areas where lineations plunge at intermediate values, kinematic indicators show a reverse/dextral oblique sense of motion. Steeply plunging lineations show both east side up shear/displacement as well as significant domains of apparent coaxial ductile strain. Regional structural and age relations suggest that the southern segment of the PKCF experienced greater overall reverse/thrust components of displacement, while the northern segment experienced a longer history of dextral displacement that coincided with the shunting in of KCF dextral motion (Nadin, 2007; Saleeby et al., this volume; Saleeby and Nadin, in prep.).

The structural evolution of the PKCF varied along its two segments. The northern segment, where it coincides with the northern KCF, follows the steeply incised N–S oriented canyon of the Kern River. The earliest brittle deformation along the northern segment is obscured by late Neogene–Quaternary normal sense remobilization (Nadin, 2007). The southern segment of the PKCF extends southward from its branching point with the KCF at 35.75° N through a series of distinct topographic saddles as it is exposed at progressively deeper levels of the oblique crustal section. Accordingly, its borders become progressively diffuse and its ductile fabrics merge with regionally pervasive, deep-crustal, high-temperature fabrics. Unlike the KCF (and coincident northern segment of the PKCF), the southern segment of the PKCF shows no evidence of having been remobilized in the late Cenozoic. However, superposed structures related to latest Cretaceous extensional modification of the Rand fault system (Wood and Saleeby, 1998; Saleeby, 2003; Maheo et al., in prep) obscure the kinematic relations along the southernmost PKCF. Structural and age relations reviewed below indicate that the ductile deformation history of the northern segment of the PKCF outlived that of the southern segment, and that dextral motion along the southern KCF replaced that of the southern PKCF as the KCF merged into the PKCF from the south.

Dextral Displacement

The dextral displacement history of the PKCF entails a complex pattern in the partitioning of motion between the principal trace of the shear zone and both the KCF and the Farewell fault zone. In order to resolve the vertical offset history of the PKCF, the subsequent dextral motion must first be backed out. We present here an overview of the constraints on the dextral displacement along the system (after Moore and du Bray, 1978; Ross, 1986; Saleeby and Busby-Spera, 1986, 1993; Busby-Spera and Saleeby, 1990; Nadin, 2007; Saleeby and Nadin, in prep). Palinspastic restoration of the dextral displacements is subsequently used as a means to better utilize disrupted spatial variation patterns of the greater SNB as markers of vertical displacement and normal shortening across the system. Figure 4 shows a summary of: 1) offset geologic markers along the system; 2) results of local dextral shear strain profiles along well-exposed transects of the shear zone (after Ramsay and Graham, 1970); and 3) a summary of principal dextral/reverse slip line orientations determined for ductile fabrics. The shear strain-derived dextral displacement values are local minimum values for the following reasons. Firstly, many of the S-C mylonites contain composite C surfaces as well as superposed high-strain shear bands. Secondly, sets of late- to post-shearing crenulations locally disrupt the principal ductile fabrics of the system. Finally, these analyses omit displacements that took place in the brittle regime as well as along fault surfaces.

We focus first on KCF dextral displacement. Based on the mapping of Ross (1986), and refinement of some of his contacts and unit designations done in conjunction with pluton geochronology (Saleeby et al., this volume) we resolve four steeply-dipping, plutonic–hypabyssal bodies that all exhibit dextral separations of 12±1 km (Fig. 4, **a–d**). In that the contacts dip steeply, both to the NE and SW, we consider this value to approximate slip. A critical relation shown on the Figure 4 Inset is that the KCF merges with the PKCF in the area where the 86–83 Ma Goldledge mylonitic granite cuts out the ca. 95 Ma Cannell Creek mylonitic granite. Both granites were ductilely sheared under solidus to hot subsolidus conditions, but the Goldledge granite cut the northern end of the Cannell Creek body following the main ductile shear phase of the latter. The Cannell Creek body shows steep east side up ductile fabrics that are both domainally overprinted and progressively transposed by ductile dextral fabrics, whereas the Goldledge body shows only pervasive ductile dextral fabrics overprinted by brittle dextral fabrics. Thus the 12±1 km of KCF dextral slip is interpreted to have been shunted at least in part into Goldledge granite ductile shear, which shows a minimum shear strain-derived dextral displacement of ~4 km (Traverse **e**, Fig. 4 Inset). The ~8 km displacement deficit is considered to have occurred both in the ductile as well as superposed brittle shear and faulting regime.

Dextral displacement in the ductile regime for pre-Goldledge and pre-KCF time is estimated as the value summed for the **a** through **c** traverses on the Figure 4 Inset. These values are used in aggregate because they appear to define a profile across the shear zone along which the cutting out of ductiley deformed rocks by subsequent brittle faulting was minimal. Additional shear strain traverses of **d** through **f** yield results suggesting comparable dextral displacements, but these are at least in part syn-Goldledge in age and are clearly bounded by brittle structures. The **a** through **c** sum of ~15 km is used provisionally below as the pre-KCF component of PKCF dextral displacement.

The map relations of Figure 4 indicate that the total resolvable dextral displacement along the northern segment of the PKCF should exceed that of the southern segment by that determined for the KCF (12±1 km). These two displacements sum to

~27 km for the northern segment of the PKCF. This value is in agreement with geological relations suggesting that the Durrwood and Fairview pendants have been differentially sheared and displaced dextrally from the western terminus of the Isabella pendant, and that unit 9 of the Needles intrusive suite may represent the shallow-level equivalent to unit 2 and some phases of unit 3 of the South Fork suite (Saleeby et al., this volume; Saleeby and Nadin, in prep.). It follows that dextral slip values of 12±1 km (southern KCF), ~15 km (southern PKCF), and ~27 km (northern PKCF/KCF) are applied to the palinspastic analysis below.

Dextral offsets along the northern KCF (where it overprints the PKCF) were estimated to decrease from ~13 km near the Durrwood pendant to as little as ~6.5 km at the northern mapped end of the system (Moore and du Bray, 1978). Later mapping by Ross (1986) refined the southern value of this range to 18±2 km. These dextral separation analyses are not in conflict with the ~27 km total dextral displacement derived above. The analyses of Moore and du Bray (1978) and Ross (1986) were based on offset plutons intruded primarily over the 89–84 Ma time interval (Chen and Moore, 1982; Saleeby et al., 1990, and this volume). These estimates thus only reflect the later, post-Cannell Creek increments of displacement. Furthermore, some of the older smaller offset plutonic bodies used by Moore and duBray (1978) are poorly constrained in original size and structural orientation, which poses a critical problem when vertical offset components are taken into account. Of potentially greater importance, however, is that an unknown but non-trivial component of dextral displacement was also shunted into the Farewell fault zone out of the northern segment of the system (Fig. 1).

Resolvable Timing of Displacements

The onset of activity along the PKCF is difficult to establish because much of its eastern wall was intruded out during its deformational history. Hence a great deal of its resolvable structural record lies within plutons that form the western margin of the Domelands intrusive suite (Fig. 2). Busby-Spera and Saleeby (1990) offer a scenario whereby dextral and subordinate vertical motions began as early as the 105–102 Ma eruption and ponding of the Erskine Canyon volcanic sequence. Structural relations between the Needles suite intrusives and the Fairview and Durrwood pendants within and adjacent to the shear zone allow for shear zone deformation prior to 101 Ma (Saleeby and

Nadin, in prep). Because the earliest history of the shear zone is so poorly recorded by observable and testable features, we focus here on the resolvable temporal relations. We return to possible earlier significant activity below in the context of alternative scenarios to our preferred integrated displacement model for the system.

Temporal relations in shear zone kinematics are well recorded in the Cannell Creek, Goldledge and western margins of the Castle Rock and Claraville members of the Domelands intrusive suite (Fig. 2; Busby-Spera and Saleeby, 1990; Nadin, 2007; Saleeby et al., this volume; Saleeby and Nadin, in prep.). The ~12 km long (ca. 95 Ma) Cannell Creek granite lies within the transition between the southern and northern segments of the shear zone. High-temperature solidus fabrics of this pluton record steep west-directed reverse-sense shear. These fabrics were partially overprinted under hot subsolidus conditions with dextral-sense shear bands (Nadin, 2007). Aureole fabrics of metamorphic pendant rocks next to the Cannell Creek body and within the shear zone preserve a similar structural chronology. Northward along the Cannell Creek body, granitic dikes and transposed intrusive sheets of the 86–83 Ma Goldledge complex cut out the Cannell Creek mylonites. To the east of the Goldledge, the 90–87 Ma Castle Rock megacrystic granite grades from mylonitic to protomylonitic to annealed mildly gneissic textures and fabrics over a ~2 km distance eastward into its interior. South of latitude ~35.45° N an ~1 km wide zone of PKCF ductile deformation along the western margin of the 90–93 Ma Claraville pluton exhibits strong high-temperature deformation fabrics that shows both east side up reverse and dextral shear components. A relative chronology in down-dip versus dextral shear is not clearly resolved in the Claraville due to large components of apparent coaxial deformation in this region. At one location a ca. 86 Ma granitic dike that shows little to no ductile deformation sharply crosscuts the deformation fabrics of the western Claraville, suggesting that ductile shear along this zone ended by 86 Ma. Thus the age–fabric relations in plutonic rocks within the PKCF show that principally down-dip ductile shearing commenced by 95 Ma. This activity was followed by principally dextral sense shearing with a modest east side up reverse component that ceased by 86 Ma along the southern shear zone segment, but persisted until at least 83 Ma along the northern segment.

The transition from down-dip reverse to predominantly dextral shear is recorded in the high-temperature subsolidus history of the Cannell Creek body. The Cannell Creek granite cooled to Ar closure temperatures in hornblende (~500° C) and biotite (~300° C) at 89 Ma and 79 Ma, respectively (Wong, 2005). Both mafic phases occur in highly annealed quartz- and feldspar-bearing blastomylonitic fabrics. Feldspars are known to weaken and deform in the ductile regime at ~500° C under typical shear zone stresses (Post and Tullis, 1999). Feldspars in the Cannell Creek granite resided in this weakened state as they cooled from solidus conditions within the initial down-dip shear field and entered the subsequent dextral shear field. This is evident in annealed textures in both the principal down-dip fabrics and in the domainal dextral shear band fabrics. We interpret the hornblende Ar closure age as the approximate shear sense transition age because feldspars were annealing during deformation in the ductile regime. The annealing in the feldspars is in turn overprinted by ductile–brittle deformation that records continued shearing during cooling to lower temperatures. The occurrence of biotite as deformed annealed grains and as seams along late-stage C-surfaces of mylonites, both in zones of domainal and penetrative dextral overprinting, suggests that low-magnitude ductile dextral shear persisted possibly as late as 79 Ma. Ages of closure of the (U-Th)/He system in both zircon and sphene throughout the region at ca. 80 Ma (Maheo et al., in prep.) further suggest that the transition into the brittle regime along the shear zone occurred at this time.

Map relations at the northern end of the PKCF–KCF system further constrain the dextral offset history of the northern segment of the system. Moore and du Bray (1978) show that the 84±1 Ma Mount Whitney–Paradise plutonic complex (Chen and Moore, 1982; Saleeby et al., 1990) is offset in a dextral sense by ~6.5 km. This offset must correspond to the later half of the KCF 12±1 km of dextral slip, because for the most part it post-dates the 86–83 Ma ductile dextral shear phase of the Goldledge mylonite, whose ductile fabric shear strain, as noted above, records a minimum of ~4 km of displacement (Fig. 4).

In summary, the resolvable temporal relations of PKCF–KCF activity indicate that east side up reverse ductile shear initiated as early as 95 Ma along the PKCF. This kinematic regime changed, or evolved, to dextral-reverse shear at ca. 90 Ma. By 86 Ma, ductile shear along the southern segment of the shear zone waned or ceased, and ductile to brittle dextral shearing of the KCF localized along a relatively narrow zone along its southern segment, and shunted into the northern segment of the PKCF as a zone of ductile shear. Between ~5–6 km of ductile dextral shear progressed between 86–84 Ma along the northern segment of the system, and then another ~6–7 km of dextral shear/slip followed. By 80 Ma, the final stages of dextral shearing had entered the brittle regime both as dispersed shear and concentrated faulting.

Constraints on Vertical and Horizontal Displacement Components

Dextral shear and slip components along the PKCF and KCF are reasonably constrained by mapping and structural analysis, as reviewed above. More cryptic, however, are the pre-dextral displacement reverse/thrust displacements that are also expressed in the ductile fabrics of the PKCF. We constrain these down-dip and related normal shortening components by compiling pertinent geochemical and petrologic data for the SNB and integrating these data with structural constraints. An important part of our compilation employs contouring procedures developed for analyzing large data sets. We summarize here data from several studies of aluminum-in-hornblende igneous barometry (Al-in-hbl), initial $^{87}Sr/^{86}Sr$ (Sr_i), and U/Pb zircon ages. Vertical displacement components are constrained by disruption of the regional patterns of Al-in-hbl barometry by the shear zone. One of our main goals in synthesizing the Sr_i as well as zircon age data are to combine these with rock compositional relations in the development of a regional primary structural model for the Cretaceous SNB, and to use deviations from this model in conjunction with the structural relations to better constrain the overall displacement patterns of the PKCF. The Al-in-hbl and Sr_i data consist of a compilation of published data (complete databases presented in Nadin, 2007) and a supplement to the pre-existing Al-in-hbl data set from our own determinations (Table 1).

Color contour plots were generated with the Geostatistical Analyst extension of ArcMap™ 9 to determine regional and local variations in Al-in-hbl pressures and Sr_i (cf. Fig. 5 for Al-in-hb). An interpolation technique was used to create a continuous data surface by using values in known locations to estimate values where no samples were taken. The contoured data surface is determined by a Kriging calculation, which is a weighted moving average method of interpolation. An input of a minimum of three data points simultaneously considered within overlapping 50 km diameter circles rendered the clearest contour patterns. For the igneous emplacement pressure map, sparser data sets from quantitative thermobarometric studies (Pickett and Saleeby, 1993; Dixon, 1995; Ague, 1997) were compared to the Al-in-hbl plot for confirmation. Once the contours were made, they were assigned a color scheme; in this study the colors are stretched (rather than classified) and range from lows in the blue tones to highs in the red tones. The same calculations and color scheme were applied to both Al-in-hbl and Sr_i data sets. In our final analysis of geochemical and petrologic data we derive a primary zonation map for the SNB for the region south of latitude 38° N, and transverse profiles for pluton emplacement pressures and U/Pb zircon ages.

Regional Igneous Barometric Patterns and Vertical Displacement Across the PKCF

Vertical displacement across the PKCF is constrained in part by estimates of magma emplacement and crystallization depth. These estimates are derived from Al-in-hbl barometry, which demonstrates empirically (Hammarstrom & Zen, 1986; Hollister et al., 1987) and experimentally (Johnson & Rutherford, 1989; Thomas & Ernst, 1990; Schmidt, 1992; Anderson & Smith, 1995; Ague, 1997) that the total Al content of calcic amphibole is linearly related to the depth of emplacement of hosting plutons. The predominance of gabbroic to tonalitic intrusive complexes along the western zone of the SNB poses a severe limitation in the application of Al-in-hbl barometry in this region. These complexes rarely contain the complete mineral assemblage of hornblende + quartz + K-feldspar + plagioclase + biotite + sphene + illmenite/magnetite that is required for the rigorous application of the barometer (Hammarstrom and Zen, 1986; Hollister et al., 1987; Johnson and Rutherford, 1989; Schmidt, 1992; Ague, 1997). Lack of hornblende also limits this technique for the sub-volcanic plutons of the Kern River suite, as well as for much of the Domelands intrusive suite. We therefore integrate the available Al-in-hbl barometric data with: 1) quantitative thermobarometric and phase relation data on contact metamorphic assemblages from pendants, where significant domains preserve equilibration textures; and 2) stratigraphic relations between subvolcanic plutons and hypabyssal–volcanic units. It is also important to note the possibility that during progressive emplacement of plutons different bodies may migrate in depth relative to one another without resetting the hornblende barometer (cf. Saleeby et al., 2003). In our samples, we looked for pristine hornblende crystals that lacked textural evidence of disturbance, such as retrograde reactions. Each emplacement pressure was determined from analyses of at least 3 hornblende grains per sample, and for each hornblende, at least 5 points were analyzed around its rim, where textural relations indicate equilibrium with quartz. We used the Schmidt (1992) calculation to determine pressure from total Al content, because of the relatively low errors associated with this calculation (± 0.6 kbar), and its use in the most recent literature (Ague, 1997; Brady et al., 2006). In addition to the errors associated with this calculation, another accuracy limitation of the technique related to the possible influence of temperature on the pressure determination (Anderson and Smith, 1995; Ague, 1997) has been noted. This possible limitation is not a major concern in our analysis, which focuses on the relative values across map-scale pressure gradients and structural breaks for rocks with a limited range of bulk composition and mineral modes. Furthermore, there is agreement (within analytical uncertainty) between Al-in-hbl determinations and data from proximal igneous and metamorphic assemblages for which quantitative thermobarometric and phase relation determinations have been made, and this agreement occurs over a broad range of determined pressures across the study area. When considered on a whole-batholith scale, the barometric data reveal regional patterns and local anomalies that are consistent with other observations.

Ague and Brimhall (1988) assessed pressure of emplacement of plutons in California batholiths, as well as regional variations in bulk chemistry, mineralogy, and mineral compositions. More focused studies have been performed within and adjacent to the study area, mostly in conjunction with quantitative thermobarometric studies of both batholithic and pendant rocks (Pickett and Saleeby, 1993; Dixon, 1995; Ague, 1997; Brady et al., 2004) We expanded on this database by sampling in the region of South Fork Valley in order to elucidate systematic local variations and their potential relationships to displacement along the transition zone between the southern and northern segments of the PKCF. Hornblende compositions of 15 new samples from granodioritic rocks were measured by electron microprobe. Eight analyses were performed on a JEOL JXA-733 and seven analyses were performed on a recently acquired JEOL JXA-8200.

Instrumental error is far outweighed by the accuracy limitations of ± 0.6 kb. The new data are presented in Table 1, and these data are added to the regional database and contoured on Figure 5. It is important to note that this compilation includes data from the Jurassic–Triassic as well as Cretaceous members of the Sierran arc. Figure 5 reveals a general west to east decrease and a north to south increase in igneous emplacement pressures. The steep north to south gradient along the southernmost region shows the oblique crustal section through the SNB. The low pressures determined for the domain along the eastern Sierra crest region are corroborated by the presence of relatively intact mid-Cretaceous silicic volcanic sections that lie unconformably on lower Mesozoic–Paleozoic pendant rocks (Fiske and Tobisch, 1994), as well as vent phases in some of the larger eastern plutons (Coleman and Glazner, 1998). An increase in pressures to as high as ~4 kb along the eastern crest centered over latitude ~37.5° N reflects emplacement pressures determined primarily in Jurassic–Triassic plutons of that area. The significance of these higher pressures in the context of the depth patterns of the Cretaceous batholith is difficult to assess.

The general eastward decrease in pressures across the Cretaceous batholith may be interpreted to mark the progressive unroofing of the older, more westerly zones of the SNB as magmatism progressed eastward through Late Cretaceous time. In terms of the higher-volume Cretaceous plutonic units, taken at east–west extremes, this would correspond to a maximum of ~3 kb of synbatholithic exhumation along the western zone over an ~25 m.y. time interval. Given a depth of exposure–igneous pressure conversion of 3.64 km overburden/kb pressure (assuming a bulk density of 2695 kg/m^3), this corresponds to an integrated exhumation rate of 0.44 mm/yr. This exhumation rate is an order of magnitude faster than that determined regionally by low-temperature thermochronological studies for the southern Sierra's post-magmatic history, stretching from latest Cretaceous time to the late Neogene uplift of the modern range (Clark et al., 2005). It is also about one order of magnitude slower than the rate determined for the initial Late Cretaceous exhumation of the southernmost SNB oblique crustal section (Saleeby et al., 2007). The faster exhumation rate in Late Cretaceous time, compared to that of latest Cretaceous to Late Neogene time, may also be correlated to the internal deformation of the SNB crust as recorded by the PKCF and other ductile shear zones that deform the central SNB (Table 2).

The north to south increase in pressures along the southern SNB occurs along different gradients in opposing walls of the PKCF. This in and of itself indicates some component of vertical displacement across the PKCF. The pressure gradient across the PKCF between latitudes ~35.2° N and 35.8° N and its attendant implication of vertical displacement form the focus of Figure 6, which is a palinspastic restoration of dextral displacements along the PKCF–KCF system keyed to the displacement constraints given in Figure 4. This restoration assumes that dextral displacement post-dated most of the vertical displacement, which is supported by the age and structural relations discussed above. Accordingly, the PKCF is shown as a west-directed reverse or thrust fault on Figure 4. Al-in-hbl barometric and available peak contact metamorphic quantitative thermobarometric data points are plotted in their restored positions. The restoration is truncated at latitude ~35.2º N because structural and age relations for the deeper-level rocks south of this area require a much more complex restoration. Most notable are that SSW-directed extension and clockwise rotation must accompany restoration of dextral slip along the southernmost KCF, and that south of the King Solomon Ridge shear zone (Fig. 2), extensional and sinistral remobilization(s) of the PKCF are a poorly constrained factor (Kanter and McWilliams, 1982; Wood and Saleeby, 1998; Saleeby et al., 2007; Maheo et al., in prep).

The first-order feature that arises from the Figure 6 restoration is an ~40 km long zone along which the Erskine Canyon volcanic sequence and its (Kern River) subvolcanic intrusives are juxtaposed across the PKCF against deeper-level rocks of the South Fork and Domelands suites. Stratigraphic and structural relations constrain formation of the volcanic and shallow intrusive sequence to within an interval of ~6 km deep to surface levels (Saleeby et al., this volume; Saleeby and Nadin, in prep.). This juxtaposition alone indicates substantial east side up displacement across the PKCF corresponding to as much as 3–4 kb. However, it ignores possible downward displacement of the Erskine Canyon sequence during intrusion of the Bear Valley and Needles suites (cf. Saleeby et al., 2003). Thus, 3–4 kb is considered a maximum possible value for the pressure jump across the shear zone. A more conservative estimate is gained by projecting the geobarometric data that are plotted on the palinspastic base within the two ENE–WSW oriented corridors shown onto profiles that traverse the PKCF (Fig. 7). The data arrays have considerable scatter, but clearly show the affects of east side up displacement. Linear regressions for each of the hanging and footwall arrays are shown as a means to interpret the data. The intersection of the footwall and hanging wall linear trends with the PKCF for the northern profile suggests an ~1.8 kb jump across the shear zone, while that of the southern profile suggests a jump of only ~0.5 kb. We provisionally favor the jump indicated by the northern profile because of the poorly constrained magnitude of extensional modification of the PKCF and its footwall in the region south of the King Solomon Ridge shear zone (Wood and Saleeby, 1998; Maheo et al., in prep.; Saleeby and Nadin, in prep.). Taking 4 kb from the Erskine Canyon suite relationships as the maximum value and 1.8 kb from the northern paleopressure profile as the minimum, and using the rock overburden conversion factor of 3.64 km/kb, we roughly constrain the east side up displacement component to within the range of ~10±5 km. We give highest confidence to this value in the South Fork Valley area, where geobarometric data are most abundant.

It is important to consider the application of the ~10±5 km value of vertical displacement across the shear zone to regions to the north and south of the South Fork Valley area. Shear zone fabrics suggest that the vertical displacement components of the shear zone diminish northward. Inspection of Figure 6 shows this to be a predicted result of the shear zone structural chronology presented earlier. At the time frame depicted in the restoration (90–95 Ma), much of the Domelands suite along the northern hanging wall area had yet to be emplaced. Thus any substantial vertical displacements across the shear zone in the area to the north occurred between the footwall and framework rocks for the younger phases of the Domelands suite that were subsequently displaced by progressive magma injection. To the south, as noted above, extensional overprints have severely complicated the analysis. In addition to the King Solomon Ridge shear zone disrupting footwall structural integrity, other extensional structures like the North Walker Basin fault (Fig. 2) have modified structural relief across the shear zone (Maheo et al., in prep.; Saleeby and Nadin, in prep.). Furthermore, we discuss evidence below suggesting that normal shortening components across the shear zone increase markedly southward towards the southern terminus of the shear zone. This leads us to suspect that vertical displacements also remained high, on the order of ~10 km, and that the apparent decrease in vertical components from the northern to the southern profile on Figure 7 is an artifact of both footwall extensional modification and possible generation of differential structural relief in footwall and hanging wall domains during initial normal shortening deformation. We now turn our attention to constraining normal shortening components across the PKCF.

Regional Spatial Variation Patterns in SNB Petrology and Geochemistry

The SNB has been well characterized in terms of regional spatial variation patterns in bulk composition, age and Sr, Nd, Pb and O isotopes. Extensive published data sets exist for Sr_i and U/Pb zircon ages. Regional spatial variation patterns in Sr_i track with isotopic variation patterns of Nd, Pb, and O, and these in general reflect geographic variation patterns in magma source regimes (cf. DePaolo, 1981; Kistler, 1990). Below we briefly review these patterns from the perspective of Sr_i, and show that they are disrupted by the PKCF. We also show that spatial variation patterns in U/Pb zircon ages are likewise disrupted by the PKCF. Pursuing the spatial variation patterns and their PKCF-related disruptions further, we develop a regional primary structural model for the SNB, and then use deviations from this model to constrain the magnitude of PKCF-related disruptions with a focus on arc normal shortening components.

Regional variation patterns in Sr_i

The application of radiogenic isotopic data to the mapping of spatial variations in magma source regimes and possible crustal assimilation components in regional composite batholiths was applied first to the SNB (cf. Kistler and Peterman, 1978; DePaolo, 1981). Since these seminal works there has been a continuously growing database of isotopes for the SNB, and for Sr_i in particular. Contouring of this Sr_i data for the SNB shows a general increase from values as low as 0.7037 in the west to as high as 0.7093 in the east (Fig. 8). This transition has been interpreted to reflect the relative contributions of different lithosphere types to the batholith source regime, with limited upper crustal contributions (cf. Kistler and Peterman, 1978; Kistler, 1990). Low Sr_i values along the west side reflect a predominance of Paleozoic oceanic lithosphere in the magma source, while higher values to the east represent significant contributions from North American continental lithosphere. The steepness of the Sr_i gradient along the west side mimics the late Paleozoic truncation zone along which Paleozoic oceanic lithosphere was emplaced by transform faulting prior to the establishment of the Mesozoic active margin (Davis et al., 1978). The Mesozoic active margin subsequently nucleated along the transform zone (Saleeby, 1981, 1992). This steep gradient also mimics fundamental structural breaks in protolith stratigraphy of western wall rocks and pendants. The wedge-shaped domain of low Sr_i values in the extreme southeast Sierra reflects plutons emplaced into a fault sliver of transitional Paleozoic lithosphere that was displaced southwards in the late Paleozoic transform truncation zone (Davis et al., 1978; Behr and Dunne, 2006).

The spatial variation patterns in Sr_i reflect pre-batholithic, lithosphere-scale structures that have been geochemically "fossilized" into the current crustal structure by large-volume magmatism. In contrast, some sharp variation patterns reflect structural modifications tectonically imposed on the primary batholithic structure. For example, the extreme westward deflection of relatively high Sr_i values along the southernmost Sierra Nevada is a result of allochthonous eastern zone SNB rocks lying in upper plates of the southern Sierra detachment system (Wood and Saleeby, 1998), generalized on Figures 2 and 3 as the Blackburn Canyon and Pastoria faults. An analogous superimposed structural modification is expressed along the southern segment of the PKCF. Close inspection of Figure 8 reveals that the $Sr_i = 0.706$ isopleth trends into the PKCF at ~35.5° N, and that these two features coincide south of this latitude. We interpret this coincidence to result from the tectonic disruption of primary batholithic structure across the PKCF. As support to this hypothesis, we present below a synthesis of U/Pb zircon age data for the southern SNB.

U/Pb Zircon Age Variation Patterns

Large data sets of U/Pb zircon ages have been published for the SNB (Saleeby and Sharp, 1980; Stern et al, 1981; Chen and Moore, 1982; Saleeby et al., 1987, 1990, 2007, and this volume). Several profiles were constructed from these and other smaller data sets across the central to southern SNB at different latitudes in order to compare trends in pluton U/Pb zircon ages (Fig. 9). The central to southern SNB was divided into four transverse corridors, and the values of concordant U/Pb zircon ages for Cretaceous plutons were projected onto their respective profiles. Also shown on these profiles are the positions of the PKCF and the possibly correlative Sierra Crest dextral shear system of the central SNB (Tikoff and Greene, 1994; Tikoff and Saint Blanquat, 1997). In the central SNB, Cretaceous magmatism migrated eastward through time at an apparent rate of ~3 mm/yr (Chen and Moore, 1982; Fig. 9a and b). This pattern is typical of the zonation for the bulk of the SNB. It is important to note that Early Cretaceous plutons occur along the eastern domains of these profiles, but, like Jurassic and Triassic plutons, these are parts of the country rock framework that were disrupted and differentially displaced during the eastward progression of higher-volume Late Cretaceous magmatism.

Inspection of profiles **a** and **b** on Figure 9 reveals that there is no disruption in the eastward-younging trend in the northern part of the batholith, even across the Sierra Crest shear system. This is not true across the PKCF. The contrasts between the age profiles of **a** and **b** versus **c** and **d** to a first order reflect the disruption of the southern SNB by the PKCF. The distinct spike in ages immediately east of the PKCF on profile **c** corresponds to the dikes and structurally concordant intrusive sheets of the Goldledge granite that were emplaced into the shear zone during the later phases of its ductile deformation history. These age data are shown as open circles, and unlike the other data points, they reflect relatively trivial volumes of magma emplacement. Otherwise, profile **c** follows the same generally smooth, eastward-younging trend of profiles **a** and **b**. Profile **d**, whose data envelop the southern ~30 km of the PKCF, exhibits a very different pattern, with a distinct age jump across the PKCF that corresponds to almost 10 m.y. of missing plutonic activity along the shear zone. This step in ages of pluton emplacement across the southern PKCF is attributed to east–west crustal shortening across the shear zone that faulted out and possibly attenuated a significant internal (axial) zone of the SNB. In order to give a more quantitative sense of the scale of this structural omission, we integrate the regional U/Pb zircon age and Sr_i data with other petrologic and structural constraints below in the development of a regional primary structural model for the SNB.

Primary Zonation of the Southern Sierra Nevada Batholith and its Disruption by the PKCF

One of the first-order structural features of the southwest Cordilleran batholithic belt is a regional transverse zonation pattern reflected in bulk composition, radiogenic isotopic compositions, and ages of pluton emplacement (cf. Moore, 1959; Silver et al., 1979; Saleeby, 1981, 2003). Profound contrasts in pendant and wall rock stratigraphic sequences also track with this zonation pattern, which typifies the Cretaceous SNB as well as the SCB and Peninsular Ranges batholith further to the south. The lithologic expression of this transverse compositional gradient in the regional batholithic belt is at regional scales a western zone rich in mafic and tonalitic rocks, an axial zone rich in tonalitic and granodioritic rocks, and an eastern zone rich in granodioritic to granitic rocks.

The co-variation in batholithic parameters outlined above can be used to divide the SNB into western, axial and eastern zones (Fig. 10). The boundary between the western and axial zones is best defined by the Sr_i=0.706 isopleth. This roughly corresponds to the ca. 100 Ma isopleth in zircon ages, and in the study area this primary boundary corresponds to the intrusive contact zone between the Bear Valley suite and the Needles and Kern River intrusive suites (Fig. 2). This boundary also roughly corresponds to the "quartz diorite boundary line" of Moore (1959). The axial zone is further defined as containing a distinct belt of pendants with remnants of mid-Cretaceous silicic metavolcanic sequences and associated hypabyssal intrusives (Burnett, 1976; Nokleberg, 1981; Saleeby et al., 1990; Kistler, 1993). In the study area, such rocks include the Kern River intrusive suite and its overlying Erskine Canyon silicic volcanic sequence. The boundary between the axial and eastern zones is defined by the western intrusive boundary of the large-volume, terminal-phase composite granitoid plutons of the eastern SNB. These large-volume plutons not only represent the youngest plutonic systems of the composite batholith, but they are petrologically, structurally and isotopically distinct. They are petrologically distinguishable from other SNB granitoids by major late phases of distinct K-feldspar megacrystic granites. Examples include the Castle Rock and parts of the Claraville plutons in the study area, and the Mount Whitney, Cathedral Peak, and Sonora Pass plutons to the north (cf. Kistler, 1993; Coleman and

Glazner, 1998). Isotopically, this belt of plutons is distinct in that its initial Pb values, which otherwise track with Sr_i through the rest of the batholith, diverge from the regional trends by decreasing eastwards (Chen and Tilton, 1991; Saleeby et al., this volume). Structurally, the eastern zone plutons are distinct in that they are bounded to the east by, and host inclusions of Jurassic and Triassic plutons (Evernden and Kistler, 1970; Stern et al., 1981; Chen and Moore, 1982). Groups of small plutons and their pendant rocks, which collectively belong to the axial zone, also occur as inclusions in the eastern zone.

The relations between the batholithic zones of Figure 10 and Late Cretaceous intra-arc ductile shear zones that are also shown on the figure shed some light on the importance of the PKCF. While central SNB shear zones such as the Bench Canyon, Long Lake, Sawmill Lake, and the composite Sierra Crest shear system do not disrupt the primary zonation pattern of the SNB, the PKCF defines a fundamental boundary along which the eastern zone truncates the axial and western zones progressively southward. We assert that this relationship reflects a profound tectonic disruption of the regional primary structure of the SNB by the PKCF. We hypothesize that this disruption includes as an important component progressively greater crustal shortening southwards along the PKCF via east side up reverse and thrust displacement. Noting that the typical across-strike width of the primary axial zone north of latitude 36° N is ~25 km, we further hypothesize that along its southern reaches as much as ~25 km of batholithic crust was faulted out along the shear zone. In our final synthesis below, we present an integrated displacement model for the PKCF–KCF system, whereby such crustal shortening is integrated with the dextral and vertical displacement components discussed above. Temporal and kinematic relations of the displacement model are compared to those of the central SNB shear zones. Finally, we present an alternative model that excludes the large crustal shortening component that is suggested by the above analysis, but which unfortunately must rely on earlier, yet to be resolved major dextral displacements along the PKCF (cf. Busby-Spera and Saleeby, 1990).

Integrated Displacement Model for the PKCF–KCF System

We have used conventional structural analysis and kinematic data to constrain dextral shear strain and displacement patterns along the PKCF–KCF system (Figs. 4 and

6), and the disruption of regional petrologic and geochemical spatial variation patterns to further constrain relative vertical displacement and possible normal shortening components across the system. General constraints on the timing of these deformation components based on geochronological data have also been reviewed. Below, we use these to develop an integrated displacement model for the system. We assume that the primary zonation pattern of the SNB, that is well preserved north of latitude ~35.5º N (Fig. 10), extended southward to and beyond the southern terminus of the SNB. Indeed, strong arguments may be offered that such a zonation pattern continued southward through the SCB, as well as the Peninsular Ranges batholith (cf. Saleeby, 2003). The alternative view, that the axial zone simply did not extend southward along the entire length of the SNB, is difficult to accept. First, this zone is clearly tectonically truncated by the PKCF (Fig. 10). Second, this view would also imply that a hiatus in magmatism of ~10 m.y. (Fig. 8d) occurred in the area coincident with the onset of an orogen-scale maxima in magmatic flux rates (Ducea, 2001; Saleeby et al., this volume). We are thus left with a profound tectonic disruption of the primary batholithic structure by the southern PKCF as the most reasonable explanation.

It is helpful to define two periods in the life of the PKCF, one clearly resolvable and one more cryptic. The resolvable history is recorded primarily within the shear zone's eastern wall Domelands intrusive suite and its pervasively deformed pendant rocks. This 95–80 Ma tectonite assemblage records various components of dextral and east side up reverse/thrust shear in its deformation fabrics. To the west, structural relations within and between the Fairview and Durrwood pendants and the Needles suite intrusives (Nadin, 2007; Saleeby and Nadin, in prep.), and to the south, structural–stratigraphic relations of the Erskine Canyon volcanic sequence (Busby-Spera and Saleeby, 1990) suggest a possible earlier deformation history along the shear zone. This cryptic history is pre-Domelands suite in age, and at least in part coincident with the 102-105 Ma eruption of the Erskine Canyon sequence. The possibility of such a cryptic deformational phase along the system leads us to consider the resolvable displacement history as possibly only the final deformational episode of the system.

Our integrated displacement analysis focuses in detail on the area shown in Figure 6, and at regional scales on Figure 10. Resolvable dextral displacement components of

~15 km along the PKCF between 95–86 Ma, and then an additional 12±1 km of dextral slip along the KCF–northern PKCF between 86–80 Ma, are given high confidence. Within the South Fork Valley area, ~10±5 km of east side up reverse shear/displacement, primarily between 95–90 Ma, is also given high confidence. This substantial vertical displacement component decreases northward along the shear zone to beyond resolution with the current data within an ~30 km distance from the South Fork Valley area. Near its southern terminus, extensional modifications have masked vertical displacement components along the shear zone. In our preferred model we interpret vertical components to have remained high southwards, in conjunction with the cutting out of the SNB axial zone. This leads us to our preferred interpretation that in its southernmost reaches the shear zone cut out perhaps as much as ~25 km of axial SNB crust in conjunction with its 95–90 Ma east side up reverse/thrust displacement phase. The correspondence of this crustal shortening phase in time with the subduction megathrust phase of displacement along the Rand fault system (discussed below), and the physical continuity of the southern PKCF with lower crustal tectonites of the Rand fault system leads us to assert that the overall displacement field proximal to the southernmost PKCF was of large enough magnitude, and of the correct kinematic sense, to drive up to ~25 km of arc-normal crustal shortening.

The realization of potential cryptic dextral displacements of substantial magnitude along the PKCF pre-dating the shear zone's resolvable history leads us to consider an alternative model for the tectonic truncation of the SNB axial zone. Hypothetical large-magnitude dextral displacements of Early Cretaceous age have been suggested for the axial SNB region (Lahren and Schweickert, 1989; Wyld and Wright, 2005). Vestiges of this older structure could be preserved within the Fairview and Durrwood Creek pendants, and within the Erskine Canyon volcanic sequence. If so, the older structure could conceivably have operated syn-magmatically within, and progressively truncated and displaced part of, the SNB axial zone. The widest reaches of the axial zone (latitudes ~36.35º N–36.9º N) could have, in this case, been tectonically widened by the strike-slip accretion of axial zone rocks displaced from the south. Such intra-batholithic dextral shearing conceivably progressed in time and space into the eastern zone terminal large-volume magmatic phase, for which many structural relations have been cited as evidence for emplacement within a dextral shear field (Saleeby, 1981; Tikoff and Saint Blanquat, 1997). This alternative model predicts that future detailed mapping within the axial zone north of 36˚ N will reveal additional dextral shear zones. As discussed below, however, such a distinct Early Cretaceous dextral shear system would require a punctuated phase of normal shortening strain across the system that intervened before the onset of the resolvable dextral shear phase of the PKCF as well as that of the Sierra crest shear zone system.

Despite the possibility of large-magnitude dextral offsets during an early cryptic phase of the PKCF history, non-trivial normal shortening components are recorded in fabrics of the shear zone where they also record east side up reverse shear between 95–90 Ma. One explanation for this is that the already existing large-magnitude strike-slip fault was highly susceptible to concentrating normal shortening strains during a 100-90 Ma regional phase of intensified normal compression, as discussed below. For some reason, shortly after this normal shortening phase along the PKCF, its southern segment became inactive and the ensuing dextral slip history routed along the KCF and northern segment of the PKCF. This profound transition of the system's behavior appears to correspond in time with a profound change in the kinematics of the Rand fault system. Between 90–86 Ma the Rand fault changed from a low-angle subduction megathrust to a regional extensional decollement system along which the underplated accretionary complex ascended back out to the southwest, presumably in a return flow channel. (Malin et al., 1995; Saleeby, 2003; Saleeby et al., 2007). At higher crustal levels above the Rand fault of the southernmost Sierra region, the Blackburn Canyon and Pastoria detachment plates (Fig. 10) were transported southwestward in response to this kinematic reversal (Wood and Saleeby, 1998; Saleeby, 2003). This is suggested to have resulted from the transfer of extensional strain into the upper crust via coupling with the regional (Rand) decollement below.

We envisage two kinematic regimes that may have worked in series, or possibly with temporal overlap, which resulted from the reversal in the principal kinematics of the Rand fault system, and which drove the coincident kinematic changes in the PKCF–KCF system. First, with the progressive lower crustal distortion of the southern PKCF as it merged with the Rand fault, its southern segment was re-oriented into an unfavorable geometry for it to efficiently partition the dextral component of oblique subduction. Figure 1 shows that the southern KCF and northern PKCF considered together trend in a more favorable orientation for playing such a kinematic role. Second, Figure 10 shows that normal-sense extensional shear and fault zones are concentrated in the panel of rocks between the KCF and the southern segment of the PKCF, and that these run at high angles to the major structures. Many, and perhaps all, of these structures began their displacement history prior to 80 Ma (Maheo et al., in prep; Saleeby and Nadin, in prep.). This leads to the possibility that the KCF and parts of the southern segment of the PKCF acted as transfer faults that bounded differentially SW-extending parts of the southernmost SNB. Such SW-directed extension in the upper plate of the Rand fault system was presumably coupled to the SW-directed return flow of the underplated accretionary complex of the Rand fault lower plate. Note also by comparing Figures 5 and 10 that the extensional structures bridging the KCF and PKCF, as well as similar structures to the northeast of the PKCF, are dispersed across the steepest gradients in pluton emplacement depths. This is consistent with arguments in favor of extensional denudation contributing significantly to the exhumation of the oblique crustal section (Malin et al., 1995; Wood and Saleeby, 1998; Saleeby, 2003; Saleeby et al., 2007). Finally, it is important to note that seismic imaging of the Rand fault system beneath the southernmost SNB shows the Rand fault dipping northward and projecting to Moho depths at latitude ~35.5º N. Thus, its northward diminishing effects on southern Sierra upper crustal structure, as implicit in the model we present above for the PKCF–KCF system, is predicted by gross crustal structure. We focus now on the broad kinematic and temporal relations of the PKCF–KCF system in comparison to other major structural systems of Cretaceous age that deformed the primary structure of the SNB.

Temporal and Kinematic Patterns of Regional Late Cretaceous Deformations of the SNB

The PKCF–KCF system lies along what may be considered a north to south regional deformation gradient in the SNB crust. To the south and continuing into the SCB, most of the Cretaceous batholith and *all* of its underlying mantle wedge are highly disrupted, or gone **(**Saleeby, 2003**)**. Batholithic rocks along the southern PKFC are highly deformed and disrupted, and along the northern PKCF are notably deformed and disrupted. Further north, the SNB is much more intact, and mantle xenolith studies indicate that its underlying mantle wedge remained intact at least through much of the Neogene (Ducea and Saleeby, 1998; Ducea, 2001; Saleeby et al., 2003). This north to south deformation gradient is also reflected by the order of magnitude increase in Late Cretaceous exhumation rates in the southernmost Sierra verses the central Sierra region that was discussed earlier. Despite the overall structural coherence of the central Sierra, numerous ductile shear zones cut the batholithic rocks of the region (Fig. 10). The regional deformation gradient in the SNB crust is a direct result of Late Cretaceous shallow slab subduction beneath the SCB and its transition into the southernmost SNB. In Table 2 we summarize what is known about the timing and kinematics of Late Cretaceous shear zones that cut the southern to central SNB. The resolvable history for the PKCF is shown first for comparison, followed by structures that record primarily arc-normal shortening strains, and finally those structures recording dextral transpression. Many of these shear zones, like the Long Lake and others that show transpressional deformation, have fabric relations like those exhibited in the Cannell Creek granite and its wall rocks, with early stage steep lineations commonly indicating east side up shear and later-stage subhorizontal lineations indicating dextral shear. In terms of temporal relations, the arc-normal shortening group was active primarily between 102–90 Ma, and locally as late as 88 Ma. Temporal constraints on the transpressional group lie primarily in the 88-80 Ma time interval.

The temporal and kinematic data summarized in Table 2 indicate an intra-arc deformational history distributed across the central SNB similar to that which is concentrated along the PKCF in the southern SNB. Most notable is a transition from predominantly arc-normal shortening with subordinate dextral transpression to predominantly dextral transpression at ca. 90 Ma, and lasting until ca. 80 Ma. Increased coupling between upper and lower subduction plates during the onset of the Laramide orogeny by Farallon slab flattening at ca. 100 Ma (cf. Dickinson and Snyder, 1978) conceivably drove arc-normal shortening across shear zones, followed and possibly compounded by an increase in subduction obliquity (Engebretsen et al., 1985) leading to the subsequent transpressional phase. These evolving subduction parameters worked in conjunction with the generation of arc magmas within an ~100 km thick fertile mantle wedge environment throughout the greater SNB (Ducea and Saleeby, 1998; Ducea, 2001; Saleeby et al., 2003). In contrast, beneath the southernmost SNB and adjacent SCB, the Farallon plate took a much shallower and flatter subduction trajectory. This led to shearing off of the respective mantle wedge and in series the underplating of an accretionary complex that was displaced down the shallow subduction zone from the Franciscan trench (Grove et al., 2003; Saleeby, 2003). Proximal to this environment, arc-normal shortening and subsequent transpression were concentrated along the PKCF. This structure appears to have emerged northward out of the Rand shallow subduction megathrust, like a crustal-scale lateral ramp, and followed northward the boundary between older solidified plutons to the west and actively growing plutons to the east. As suggested by Tikoff and Green (1994) and Tikoff and Saint Blanquat (1997), the northern PKCF may have stepped eastward into the magmatically active eastern batholithic zone to join the transpressional shear zones that link up to form the Sierra Crest shear system (Fig. 10), but this is yet to be firmly documented. Finally, the relations summarized in Table 2 have important implications for the possible early history of the PKCF, if large cryptic dextral displacements are to be invoked for the truncation of the SNB axial zone. The initial resolvable east side up reverse/thrust history of the system, post-dating the cryptic history, in this case reflects the shear zone's response to the same intensified normal compression pulse to which the Quartz Mountain, Kaiser Peak, Courtright-Wishon, Long Lake, and Sawmill Lake shear zones appear to have responded. Immediately thereafter, the PKCF resumed its dextral transpression history coincident with that of the Sierra Crest shear system.

Summary and conclusions

In the southern SNB, a regional ductile shear zone, the PKCF, localized along a zone that separates Late Cretaceous plutons to the east from Early to mid-Cretaceous plutons to the west. Shear zone activity progressed while the Late Cretaceous plutons were emplaced and cooled from solidus to hot subsolidus conditions. Conventional structural analysis resolves a dextral displacement of ~27 km along the northern segment of the shear zone. To the south, such displacement was partitioned into an ~15 km component along the southern segment of the shear zone, and an ~12±1 km component along the KCF, a southward-projecting ductile–brittle branch that extends southwestward from the composite PKCF–KCF system to the north. The southern segment of the PKCF exhibits early fabrics indicating substantial east side up reverse shear/displacement overprinted by fabrics indicating oblique dextral–reverse shear and subsequent dextral shear. Fabrics along the northern branch exhibit primarily dextral shear with minor east side up reverse components. Ductile deformation began along the shear zone by 95 Ma, appears to have ceased or waned substantially along the southern segment by 86 Ma, and persisted along the northern segment in conjunction with KCF dextral motion until ca. 80 Ma.

Despite being able to constrain the dextral displacement history of the shear zone to a reasonable degree of confidence by conventional structural analysis, geologic markers that could constrain vertical displacements, as well as horizontal shortening components across the shear zone, are less obvious. We utilize large data sets in igneous (Al-in-hb) barometry, U/Pb zircon ages, and Sr_i to help constrain these deformational components. The igneous barometric data, when coupled with other barometric systems and pendant stratigraphic relations, suggest ~10±5 km of east side up vertical throw along the southern segment and its transition into the northern segment of the shear zone. Vertical throw diminishes northward in concert with the apparent disappearance of vertical shear deformation fabrics. The Sr_i data, when integrated with pluton petrologic and age data, and pendant stratigraphy, define distinct longitudinal zones of the SNB that are continuous at regional scales. Evidence of significant east–west shortening across the southern segment of the PKCF is manifest in the truncation of the otherwise regionally continuous axial zone of the batholith. Such shortening may have consumed up to ~25 km of crust along the southern segment of the shear zone, and appears to have occurred in conjunction with the east side up vertical throw resolved in the geobarometric data. The initial west-directed ductile reverse/thrust displacement phase along the PKCF changed to primarily dextral strike-slip shearing at ca. 90 Ma. A similar change from arc-normal shortening to dextral transpression is recorded at ca. 90 Ma in ductile shear zones that are widely dispersed in the central SNB. This change may be correlated to the Farallon plate subduction trajectory becoming increasingly oblique and the resulting tangential strain component being partitioned into the SNB along ductile shear zones. In contrast to the central SNB shear zones, which dispersed intra-arc deformation across the region, the PKCF guided both arc-normal shortening and subsequent transpression along a much more concentrated zone. This reflects yet another mid-Cretaceous change in subduction parameters, in this case affecting primarily the southernmost SNB. In the southernmost SNB and the adjacent SCB, a change in the dip of the underlying subducting Farallon plate to a shallow trajectory in Late Cretaceous time led to intensified intra-arc deformation and to the unroofing of an oblique crustal section. Early-stage reverse/thrust displacements across the PKCF appear to have been kinematically linked to the shallowing of the Farallon slab. Later-stage dextral shearing appears to have been coincident with regional transpression across much of the axial to eastern zones of the SNB that arose in response to increasing dextral components in oblique subduction. Latest-stage dextral displacements may have been at least partly coupled to the extensional denudation that unroofed the southern SNB oblique crustal section.

Acknowledgements

This study benefited from contributions and interactions with Jay Ague and Rob Brady. Helpful reviews of an earlier version of this manuscript by C.G. Barnes and P.H. Wetmore are kindly acknowledged. Assistance with microprobe analyses and Al-in-hbl data interpretation from Chi Ma, Peter Luffi, and Laura Baker is greatly appreciated, as is software help from Nathan Niemi, JoAnne Giberson, and Ryan Petterson. Assistance with drafting from Zorka Saleeby is kindly acknowledged. Discussions of Sierra Nevada batholith shear zones with Basil Tikoff were also illuminating. This research was partly supported by NSF grant EAR0230383, and a grant from the Gordon and Betty Moore Foundation. The second author acknowledges C.A. Hopson for his inspiration to integrate the fields of tectonics and petrology. Caltech Tectonics Observatory contribution number 51.

References

Ague, J., 1997, Thermodynamic calculation of emplacement pressures for batholithic rocks, California; implications for the aluminum-in-hornblende barometer: Geology, v. 25, no. 6, p. 563.

Ague, J., and Brimhall, G. H., 1988, Magmatic arc asymmetry and distribution of anomalous plutonic belts in the batholiths of California - effects of assimilation, crustal thickness, and depth of crystallization: Geological Society of America Bulletin, v. 100, no. 6, p. 912-927.

Anderson, J. L., and Smith, D. R., 1995, The effects of temperature and f_{O2} on the Al-in-hornblende barometer: The American Mineralogist, v. 80, no. 5, p. 549.

Behr, W., and Dunne, G. C., 2006, Evidence for multiple strands of the Late Paleozoic truncational fault of North America within exposures of the Kennedy Meadows pendant: Sierra Nevada, CA: Abstracts with programs - Geological Society of America, Cordilleran section.

Brady, R. J., Ducea, M. N., Kidder, S. B., and Saleeby, J. B., 2004, The distribution of radiogenic heat production as a function of depth in the Sierra Nevada Batholith, California: Lithos, v. 86, p. 229-244.

Burnett, J.L., 1976, Kaweah Peaks pluton and its relationship to the age of the Kern Canyon fault, Tulare County, California: California Division of Mines and Geology, Map Sheet 35, scale 1:62,500, 7 pp text.

Busby-Spera, C.J., and Saleeby, J.B., 1987, Geologic guide to the Mineral King area, Sequoia National Park, California: The Pacific Section Society of Economic Paleontologists and Mineralogists, Los Angeles, California, v. 56, 44 pp.

Busby-Spera, C.J., and Saleeby, J.B., 1990, Intra-arc strike-slip fault exposed at batholithic levels in the southern Sierra Nevada, California: Geology, v. 18, no. 3, p. 255-259.

Cheadle, M. J., Czuchra, B. L., Byrne, T., Ando, C. J., Oliver, J. E., Brown, L. D., Kaufman, S., Malin, P. E., and Phinney, R. A., 1986, The deep crustal structure of the Mojave Desert, California, from COCORP seismic reflection data: Tectonics, v. 5, no. 2, p. 293.

Chen, J. H., and Moore, J. G., 1982, Uranium-Lead isotopic ages from the Sierra Nevada batholith, California: Journal of Geophysical Research, v. 87, no. B6, p. 4761-4784.

Chen, J. H., and Tilton, G. R., 1991, Applications of lead and strontium isotopic relationships to the petrogenesis of granitoid rocks, central Sierra Nevada batholith, California: Geological Society of America Bulletin, v. 103, p. 439-447.

Clark, M. K., Maheo, G., Saleeby, J., and Farley, K. A., 2005, The non-equilibrium landscape of the southern Sierra Nevada, California: GSA Today, v. 15, no. 9, p. 4-10.

Clemens-Knott, D., and Saleeby, J.B., 1999, Impinging ring dike complexes in the Sierra Nevada batholith, California: Roots of the Early Cretaceous volcanic arc: Geological Society of America Bulletin, v. 111, no. 4, p. 484-496.

Coleman, D.S., and Glazner, A.F., 1998, The Sierra crest magmatic event: rapid formation of juvenile crust during the late Cretaceous in California, Integrated Earth and Environment Evolution of the Southwestern United States, Ed. W. G. Ernst and C. A. Nelson, 253-272.

Coleman, D. S., Gray, W., and Glazner, A. F., 2004, Rethinking the emplacement and evolution of zoned plutons; geochronologic evidence for incremental assembly of the Tuolumne Intrusive Suite, California: Geology, v. 32, no. 5, p. 433.

Davis, G. A., Monger, J. W. H., and Burchfiel, B. C., 1978, Mesozoic construction of the Cordilleran "collage", central British Columbia to central California, *in* Howell, D. G., and McDougall, K. A., eds., Mesozoic paleogeography of the western United States: Los Angeles, California, Pacific Section Society of Economic Paleontologists and Mineralogists Pacific Coast Paleogeography Symposium 2, p. 1-32.

Davis, M., Teyssier, C., and Tikoff, B., 1995, Dextral shearing in the Cascade Lake shear zone, Tuolumne intrusive suite, Sierra Nevada, California: Abstracts with programs - Geological Society of America, v. 6, p. 222.

DePaolo, D. J., 1981, A neodymium and strontium isotopic study of the Mesozoic calc-alkaline granitic batholiths of the Sierra Nevada and Peninsular Ranges, California: Journal of Geophysical Research B, v. 86, no. 11, p. 10470.

Dickinson, W. R., and Snyder, W. S., 1978, Plate tectonics of the Laramide Orogeny, *in* Matthews, V., III, ed., Laramide folding associated with basement block faulting in the western United States, Geological Society of America Memoir, Geological Society of America (GSA), Boulder, CO, United States (USA), p. pp.355-366.

Dixon, E. T., 1995, An evaluation of hornblende barometry, Isabella to Tehachapi region, southern Sierra Nevada, California: MS Thesis, University of Michigan, 150 pp.

du Bray, E.A., and Dellinger, D.A., 1981, Geologic map of the Golden Trout Wilderness, southern Sierra Nevada, California: U.S. Geological Survey Miscellaneous Field Studies Map MF-1231-A, 1:48,000.

Ducea, M. N., 2001, The California Arc: Thick granitic batholiths, eclogitic residues, lithospheric-scale thrusting, and magmatic flare-ups: GSA Today, v. 11, no. 11, p. 4-10.

Ducea, M. N., and Saleeby, J. B., 1998, The age and origin of a thick mafic-ultramafic keel from beneath the Sierra Nevada batholith: Contributions to Mineralogy and Petrology, v. 133, p. 169-185.

Engebretson, D. C., Cox, A., and Gordon, R.G., 1985, Relative motions between oceanic and continental plates in the Pacific Basin: Geological Society of America Special Paper, v. 206, 59 pp.

Evernden, J. F., and Kistler, R. W., 1970, Chronology of emplacement of Mesozoic batholithic complexes in California and western Nevada: U. S. Geological Survey Professional Paper, Report P 0623, p. 42 pp.

Fiske, R. S., and Tobisch, O. T., 1994, Middle Cretaceous ash-flow tuff and caldera-collapse deposit in the Minarets Caldera, east-central Sierra Nevada, California: Geological Society of America Bulletin, v. 106, no. 5, p. 582-593.

Giorgis, S., Tikoff, B., and McClelland, W., 2005, Missing Idaho arc: Transpressional modification of the $^{87}Sr/^{86}Sr$ transition on the western edge of the Idaho batholith: Geology, v. 33, no. 6, p. 469-472.

Greene, D.C., and Dutro, T.J., 1991, Stratigraphic affinity and structural implications of late Paleozoic fossils in the Ritter Range pendant, eastern Sierra Nevada, California: Abstracts with programs - Geological Society of America, v. 23, n. 2, p. 30.

Greene, D. C., and Schweickert, R. A., 1995, The Gem Lake shear zone; Cretaceous dextral transpression in the northern Ritter Range pendant, eastern Sierra Nevada, California: Tectonics, v. 14, no. 4, p. 945-961.

Grove, M., Jacobson, C. E., Barth, A. P., and Vucic, A., 2003, Temporal and spatial trends of Late Cretaceous-early Tertiary underplating Pelona and related schist beneath Southern California and southwestern Arizona: Special Paper - Geological Society of America, v. 374, p. 381-406.

Gutscher, M. A., 2001, An Andean model of interplate coupling and strain partitioning applied to the flat subduction zone of SW Japan (Nankai Trough): Tectonophysics, v. 333, no. 1-2, p. 95-109.

Hammarstrom, J. M., and Zen, E.-A., 1986, Aluminum in hornblende: an empirical igneous geobarometer: American Mineralogist, v. 71, no. 11-12, p. 1297-1313.

Hathaway, G. M., and Reed, W. E., 1994, The Long Lake shear zone; implications for dextral sense shear zones in the Sierra Nevada Batholith, east-central California: Abstracts with programs - Geological Society of America, v. 26, no. 7, p. 385.

Hollister, L. S., Grissom, G. C., Peters, E. K., Stowell, H. H., and Sisson, V. B., 1987, Confirmation of the empirical correlation of Al in hornblende with pressure of solidification of calc-alkaline plutons: The American Mineralogist, v. 72, no. 3-4, p. 231-239.

Jarrard, R. D., 1986, Causes of compression and extension behind trenches: Tectonophysics, v. 132, no. 1-3, p. 89-102.

Jayko, A. S., and Blake, M. C., Jr., 1993, Northward displacements of forearc slivers in the Coast Range of California and southwest Oregon during the late Mesozoic and early Cenozoic, *in* Dunne, G., and McDougall, K., eds., Mesozoic Paleogeography of the western United States-II: Pacific Section Society of Economic Paleontologists and Mineralogists, Book 71, p. 19-36.

Johnson, M. C., and Rutherford, M. J., 1989, Experimental calibration of the aluminum-in-hornblende geobarometer with application to Long Valley Caldera (California) volcanic rocks: Geology, v. 17, no. 9, p. 837-841.

Kanter, L.R., and McWilliams, M.O., 1982, Rotation of the southernmost Sierra Nevada, California: Journal of Geophysical Research, v. 87, p. 3819-3830.

Kelley, K. P., and Engebretson, D. C., 1994, Updated relative motions and terrane trajectories for North America and oceanic plates; Cretaceous to present: Abstracts with programs - Geological Society of America, v. 26, no. 7, p. 459.

Kistler, R. W., 1990, Two different lithosphere types in the Sierra Nevada, California: Memoir - Geological Society of America, v. 174, p. 271-281.

Kistler, R.W., 1993, Mesozoic intrabatholithic faulting, Sierra Nevada, California, *in* Dunne, G. C., ed., Mesozoic paleogeography of the Western United States-II: Pacific Section, Society of Economic Paleontologists and Mineralogists, Book 71, p. 247-260.

Kistler, R. W., and Peterman, Z. E., 1978, Reconstruction of crustal blocks of California on the basis of initial strontium isotopic compositions of Mesozoic granitic rocks, U.S. Geological Survey Professional Paper 1071, 17 pp.

Kistler, R. W., and Ross, D. C., 1990, A strontium isotopic study of plutons and associated rocks of the southern Sierra Nevada and vicinity, California: U.S. Geological Survey Bulletin 1920, 20 pp.

Kistler, R. W., and Champion, D. E., 2001, Rb-Sr whole-rock and mineral ages, K-Ar, ^{40}Ar/ ^{39}Ar, and U-Pb mineral ages, and strontium, lead, neodymium, and oxygen isotopic compositions for granitic rocks from the Salinian Composite Terrane, California: Open-File Report - U. S. Geological Survey, Report: OF 01-0453, 83 pp.

Lahren, M. M., and Schweickert, R. A., 1989, Proterozoic and Lower Cambrian miogeoclinal rocks of Snow Lake Pendant, Yosemite-Emigrant Wilderness, Sierra Nevada, California; evidence for major Early Cretaceous dextral translation: Geology, v. 17, no. 2, p. 156-160.

Li, Y.-G., Henyey, T. L., and Silver, L. T., 1992, Aspects of the crustal structure of the western Mojave Desert, California, from seismic reflection and gravity data: Journal of Geophysical Research B, v. 97, no. 6, p. 8805-8816.

Mahan, K. H., Bartley, J. M., Coleman, D. S., Glazner, A. F., and Carl, B. S., 2003, Sheeted intrusion of the synkinematic McDoogle Pluton, Sierra Nevada, California: Geological Society of America Bulletin, v. 115, no. 12, p. 1570-1582.

Maheo, G., Saleeby, J.B., and Farley, K.A., in prep., (U-Th)/He apatite and zircon thermochronology of the southern Sierra Nevada, California: to be submitted to Earth and Planetary Sciences Letters.

Malin, P. E., Goodman, E. D., Henyey, T. L., Li, Y. G., Okaya, D. A., and Saleeby, J. B., 1995, Significance of Seismic Reflections beneath a Tilted Exposure of Deep Continental-Crust, Tehachapi Mountains, California: Journal of Geophysical Research – Solid Earth, v. 100, no. B2, p. 2069-2087.

McLaughlin, R. J., Blake, M. C., Jr., Griscom, A., Blome, C. D., and Murchey, B. L., 1988, Tectonics of formation, translation, and dispersal of the Coast Range Ophiolite of California: Tectonics, v. 7, no. 5, p. 1033-1056.

Moore, J. G., 1959, The quartz diorite boundary line in the western United States: The Journal of Geology, v. 67, no. 2, p. 198-210.

Moore, J. G., and du Bray, E., 1978, Mapped offset on the right-lateral Kern Canyon fault, southern Sierra Nevada, California: Geology, v. 6, no. 4, p. 205-208.

Nadin, E.S., 2007, Structure and history of the Kern Canyon fault system, southern Sierra Nevada, California: PhD Thesis, California Institute of Technology, 297 pp.

Nadin, E. S., and Saleeby, J. B., 2001, Relationships between the Kern Canyon Fault (KCF) and the Proto-Kern Canyon Fault (PKCF), Southern Sierra Nevada, CA: EOS, Transactions, American Geophysical Union, Fall Meeting Suppl., Abstract T32B-0902, v. 82, no. 47.

Nadin, E. S., and Saleeby, J. B., 2004, Localization of shear along a compositional discontinuity: the Proto-Kern Canyon Fault, Sierra Nevada, California: Abstracts with programs - Geological Society of America, v. 36, no. 5, p. 435.

Nokleberg, W.J., 1981, Stratigraphy and structure of the Strawberry Mine Roof Pendant, Central Sierra Nevada, California: U.S. Geological Survey Professional Paper 1154, 18 pp., 2 plts.

Pickett, D. A., and Saleeby, J. B., 1993, Thermobarometric constraints on the depth of exposure and conditions of plutonism and metamorphism at deep levels of the Sierra Nevada batholith, Tehachapi Mountains, California: Journal of Geophysical Research-Solid Earth, v. 98, no. B1, p. 609-629.

Pickett, D.A., and Saleeby, J.B., 1994, Nd, Sr, and Pb isotopic characteristics of Cretaceous intrusive rocks from deep levels of the Sierra Nevada batholith, Tehachapi Mountains, California: Contributions in Mineralogy and Petrology, v. 118, p. 198–205.

Post, A., and Tullis, J., 1999, A recrystallized grain size piezometer for experimentally deformed feldspar aggregates: Tectonophysics, v. 303, no. 1-4, p. 159-173.

Ramsay, J. G., and Graham, R. H., 1970, Strain variation in shear belts: Canadian Journal of Earth Sciences, v. 7, p. 786-813.

Ross, D. C., 1986, Basement–rock correlations across the White Wolf–Breckenridge–southern Kern Canyon fault zone, southern Sierra Nevada, California: U. S. Geological Survey Bulletin, Report B 1651, 25 pp.

Saleeby, J. B., 1981, Ocean floor accretion and volcanoplutonic arc evolution of the Mesozoic Sierra Nevada, California, *in* Ernst, W. G., ed., Rubey volume on the Geotectonic Development of California: Englewood Cliffs, N.J., Prentice-Hall, p. 132-181.

Saleeby, J. B., 1992, Petrotectonic and paleogeographic settings of U.S. Cordilleran ophiolites, *in* Burchfiel, B. C., Lipman, P. W., and Zoback, M. L., eds., The Cordilleran Orogen: Conterminous U.S.: The Geology of North America: Boulder, CO, Geological Society of America, p. 653-682.

Saleeby, J.B., 2003, Segmentation of the Laramide Slab – evidence from the southern Sierra Nevada region: Geological Society of America Bulletin, v. 115, no. 6, p. 655-668.

Saleeby, J.B., and Sharp, W., 1980, Chronology of the structural and petrologic development of the southwest Sierra Nevada foothills, California - summary: Geological Society of America Bulletin, v. 91, no. 6, p. 317-320.

Saleeby, J.B. and 12 contributors, 1986, Continent-Ocean Transect, Corridor C2, Monterey Bay offshore to the Colorado Plateau: Geological Society of America Map and Chart Series TRA C2, 2 sheets, scale 1:500,000, 87 pp.

Saleeby, J. B., Busby-Spera, C. J., 1986, Fieldtrip guide to the metamorphic framework rocks of the Lake Isabella area, southern Sierra Nevada, California, in Dunne, G. C., ed., Mesozoic and Cenozoic structural evolution of selected areas, east-central California, Geol. Soc. Am., Cordilleran Sect., Los Angeles, CA, United States (USA), p. 81-94.

Saleeby, J.B., Hannah, J. L., and Varga, R. J., 1987, Isotopic age constraints on Middle Paleozoic deformation in the northern Sierra Nevada, California: Geology, v. 15, no. 8, p. 757-760.

Saleeby, J.B., Sams, D.B., and Kistler, R.W., 1987, U/Pb zircon, strontium, and oxygen isotopic and geochronological study of the southernmost Sierra Nevada batholith, California: Journal of Geophysical Research, v. 92, p. 10,443-10,446.

Saleeby, J. B., Kistler, R. W., Longiaru, S. J., Moore, J. G., and Nokleberg, W. J., 1990, Middle Cretaceous silicic metavolcanic rocks in the Kings Canyon area, central Sierra Nevada, California: Memoir - Geological Society of America, v. 174, p. 251-270.

Saleeby, J. B., and Busby, C. J., 1993, Paleogeographic and tectonic setting of axial and western metamorphic framework rocks of the southern Sierra Nevada, California, *in* Dunne, G., and McDougall, K., eds., Mesozoic paleogeography of the western United States—II: SEPM (Society for Sedimentary Geology), Pacific Section, Book 71, p. 197–226.

Saleeby, J. B., Ducea, M. N., and Clemens-Knott, D., 2003, Production and loss of high-density batholithic root, southern Sierra Nevada, California: Tectonics, v. 22, p. n.6, doi:10.1029/2002TC001374.

Saleeby, J. B., Farley, K. A., Kistler, R. W., and Fleck, R., 2007, Thermal evolution and exhumation of deep-level batholithic exposures, southernmost Sierra Nevada, California: *in* Cloos, M., Carlson, W.D., Gilbert, M.C., Liou, J.G., and Sorensen, S.S., eds., Convergent Margin Terranes and Associated Regions: A Tribute to W.G. Ernst: Geological Society of America Special Paper 419, p. XXX-XXX, doi:10.1130/2007.2419(XX).

Saleeby, J.B., and Nadin, E.S., in prep., Structure and tectonics of the Kern Canyon fault system, California: to be submitted to Tectonics.

Schmidt, M. W., 1992, Amphibole composition in tonalite as a function of pressure; an experimental calibration of the Al-in-hornblende barometer: Contributions to Mineralogy and Petrology, v. 110, no. 2-3, p. 304-310.

Silver, L. T., Taylor, H.P. Jr., and Chappell, B., 1979, Some petrological, geochemical, and geochronological observations of the Peninsular Ranges batholith near the international border of the U.S.A. and Mexico, *in* Abbott, P.L., and Todd, V.R., eds., Mesozoic crystalline rocks–Peninsular Ranges batholith, pegmatites and Point Sal ophiolite: Geological Society of America Annual Meeting Field Trip Guide, p. 83-110.

Silver, L. T., and Mattinson, J. M., 1986, "Orphan Salinia" has a home: Eos, Transactions, American Geophysical Union, v. 67, no. 44, p. 1215.

Stern, T. W. Bateman, P.C., Morgan, B.S., Newell, M.F., Peck, D.L., 1981, Isotopic U-Pb ages of zircon from the granitoids of the central Sierra Nevada, California: U.S. Geological Survey Professional Paper, v. 1185, 17 pp.

Stock, J., and Molnar, P., 1988, Uncertainties and implications of the Late Cretaceous and Tertiary position of North America relative to the Farallon, Kula, and Pacific plates: Tectonics, v. 7, no. 6, p. 1339-1384.

Thomas, W. M., and Ernst, W. G., 1990, The aluminum content of hornblende in calc-alkaline granitic rocks; a mineralogic barometer calibrated experimentally to 12 kbars: Special Publication - Geochemical Society, v. 2, p. 59-63.

Tikoff, B., and Greene, D. C., 1994, Transpressional deformation within the Sierra Crest shear zone system, Sierra Nevada, California (92-80 Ma); vertical and horizontal stretching lineations within a single shear zone: Abstracts with programs - Geological Society of America, v. 26, no. 7, p. 385.

Tikoff, B., and Saint Blanquat, M., 1997, Transpressional shearing and strike-slip partitioning in the Late Cretaceous Sierra Nevada magmatic arc, California: Tectonics, v. 16, no. 3, p. 442-459.

Tobisch, O. T., Saleeby, J. B., Renne, P. R., McNulty, B., and Tong, W. X., 1995, Variations in deformation fields during development of a large-volume magmatic arc, central Sierra Nevada, California: Geological Society of America Bulletin, v. 107, no. 2, p. 148-166.

Wong, M. S., 2005, Structural evolution of mid-crustal shear zones: Integrated field and thermochronologic studies of the Sierra Mazatalan metamorphic core complex, Sonora, Mexico and the Proto-Kern Canyon dextral shear zone, southern Sierra Nevada, California: PhD Thesis, University of California, Santa Barbara, 175 pp.

Wood, D. J. and Saleeby, J. B. 1998, Late Cretaceous-Paleocene extensional collapse and disaggregation of the southernmost Sierra Nevada batholith: International Geology Review; v. 39, p. 973-1009.

Wyld, S. J., and Wright, J. E., 2005, New evidence for Cretaceous strike-slip faulting in the U.S. Cordillera; and implications for terrane displacement, deformation patterns and plutonism: American Journal of Science, v. 301, p. 150-181.

Yan, Z., Clayton, R. W., and Saleeby, J. B., 2005, Seismic refraction evidence for steep faults cutting highly attenuated continental basement in the central Transverse Ranges, California: Geophysical Journal International, v. 160, p. 651-666.

Figures

1. Map of southern California, showing geologic features discussed in the text. Of particular interest are the Mesozoic granitic rocks of the Sierra Nevada and associated Peninsular Ranges batholith, Salinia, and Mojave Desert (comprising the southern California Batholith, or SCB), and pendant rocks. Remnants of the Rand schist and associated schists, and the greater Franciscan complex, are also highlighted. The Proto-Kern Canyon fault and Kern Canyon fault are shown transecting the southern part of the SNB, and truncating the Sr_i = 0.706 isopleth. The Farewell fault branches out of the northern part of the KCF.

2. Map outlines of individual plutons forming the intrusive suites of the southern SNB referred to in the text. In general, the older Kern River (K), Bear Valley (B), and Needles (N) suites lie to the west of the Proto-Kern Canyon and Kern Canyon faults, while the younger South Fork (S) and Domelands (D) suites lie to the east. Critical rock fabrics that constrain early and later motion along the fault system are in the Granite of Cannell Creek (D3) and its associated Goldledge member. Also labeled are the Durrwood, Fairview, Cannell Creek, and Isabella pendants, which lie along and are disrupted by the PKCF. At its southernmost extent, the PKCF merges with the Eastern Tehachapi shear zone, and this system is truncated to the south by the Garlock fault. The Rand schist and upper plate tectonites are shown in windows adjacent to the Garlock fault, and the locations of the King Soloman Ridge shear zone and the North Walker Basin fault are also shown.

3. Cross sections across the PKCF, from north to south, showing its shallowing dip southward and eventual transition into the Rand fault. A) Near latitude 35.8˚ N, the PKCF is steep and localized along the western edge of the Domelands intrusive suite. Pendant rocks, shown in dark gray, are also highly sheared. B) Near latitude 35.4˚ N, the dip of the PKCF shallows eastward, and the KCF branches from it to the west. The shear zone is again localized along the western edge of the Domelands intrusive suite. C) Near latitude 35˚ N, the dip of the PKCF shallows further and roots into upper plate tectonites of the Rand fault. The Blackburn Canyon detachment is shown placing younger,

shallower-level Late Cretaceous upper plate intrusive rocks against lower plate intrusive rocks, which are in turn in fault contact with the Rand schist.

4. Detailed map of central region of figure 2, showing dextral separations on Kern Canyon fault (KCF) (modified after Ross, 1986) and Inset Map showing locations of traverses along which shear strain was analyzed (after Ramsay and Graham, 1970). Also shown are dextral displacement components as well as principal slip lines determined in this study for transition zone between southern and northern segments of PKCF. Selected plutons are colored to elucidate their displacement patterns along the system. Pluton unit symbols are as on Figure 2.

5. Contour plot of igneous emplacement pressures for autochthonous batholithic rocks, determined from Al-in-hbl measurements (outlined in black: allochthonous batholithic rocks of the Blackburn Canyon fault (Wood and Saleeby, 1998) and batholithic exposures south of the Garlock fault). In general, values decrease from west to east and increase from north to south, but this pattern is complicated in the southern part of the batholith in the vicinity of the PKCF. All data and sample locations are presented in Nadin (2007), and new data are presented in Table 1.

6. Palinspastic restoration of dextral displacements along KCF and shear strains along PKCF based on Figure 4 structural relations. Color scheme is same as Figure 4, except pink region shows area where Goldledge and Castle Rock members of Domelands suite will be emplaced during dextral displacement post-dating this view. Plotted on this map are the derivative locations of igneous and peak contact metamorphic barometric determinations (after Ague and Brimhall, 1988; Dixon, 1995; Brady et al., 2004; and this study). Corridors show grouping of barometric data points used for profiles of Figure 7. Sample locations given in Appendix 1.

7. Igneous and peak contact metamorphic pressure profiles across the KCF–PKCF system with dextral displacements and shear strains restored, as shown on Figure 6. Data groupings of northern and southern profiles are shown on corridors of Figure 6, and

locations listed in Appendix 1. Linear regressions through points west and east of the PKCF show in the northern profile a suggest ~1.8 kb east side up displacement across the PKCF. In the southern profile, displacement is ~0.5 kb.

8. Contour plot of Sr_i ratios in the southern half of the batholith. In general, Sr_i ratios increase from west to east, but this pattern is disrupted in the southernmost part of the batholith in the by the PKCF. Sr_i ratios and sample locations, with references, are presented in Nadin (2007).

9. Zircon U/Pb ages plotted as a function of distance across the Sierra Nevada batholith. Between latitudes A) 38˚ N to 37˚ N; B) 37˚ N to 36.5˚ N; and C) 36.5˚ N to 35.5˚, zircon U/Pb ages follow a general, eastward-younging trend of 2.7 mm/yr (Chen and Moore, 1982). Across the PKCF, between latitudes D) 35.5˚ N to 34.9˚ N, the greater SNB trend is disrupted. In A), B), and C), the greater Sierra Crest shear system and related smaller shear zones seem passively marked in progressive intrusions, while to the south, along D), the PKCF seems to actively disrupt the batholith during the youngest stages of intrusive activity. Open circles in profile C) are dikes and small tabular intrusives of the Goldledge granite. (Saleeby and Sharp, 1980; Stern et al., 1981; Chen and Moore, 1982; Chen and Tilton, 1991; Saleeby et al., 1987, 1990, 2007, this volume; Pickett and Saleeby, 1994; Tobisch et al., 1995; Clemens-Knott and Saleeby, 1999; Coleman et al., 2004).

10. Primary zonation of the Sierra Nevada batholith, and Late Cretaceous shear zones related to the PKCF. Northern and southern segments of the PKCF, and the northwest-striking Farewell fault are delineated. The Blackburn Canyon and Pastoria faults are proposed to be detachment faults that brought upper crustal batholithic rocks to their present positions above deeper-level rocks (Wood and Saleeby, 1998).

Tables

1. Average of rim analyses of hornblende from plutonic complexes of the southern SNB. Cations calculated on the basis of 23 O. Pressures calculated using the equation of Schmidt (1992).

2. Summary of ages and kinematics of central Sierra shear zones.

Appendix

1. Values, sample locations, and references for igneous and peak metamorphic pressures of samples shown in Figure 6 corridors and Figure 7 profiles.

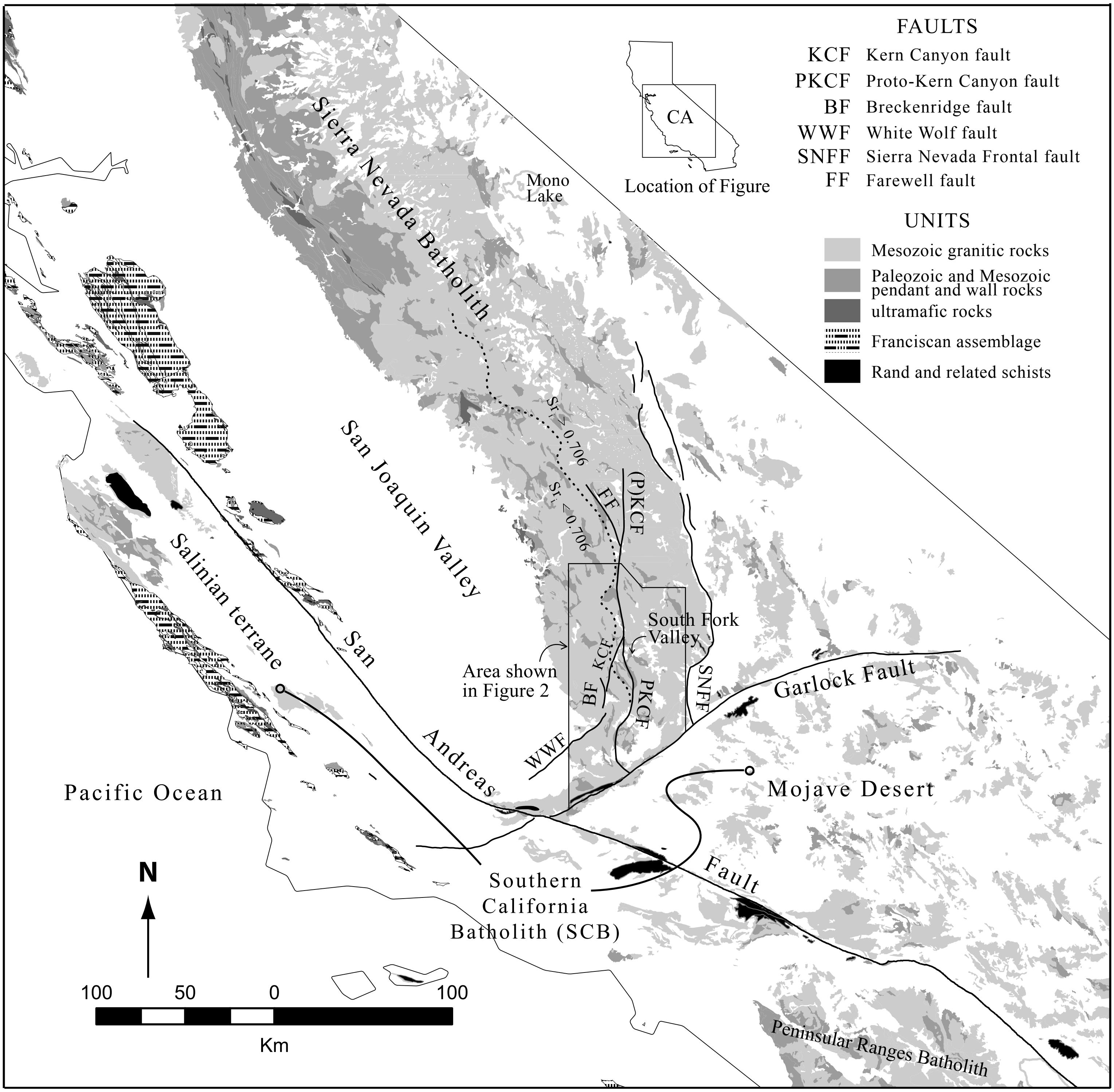
FAULTS
KCF Kern Canyon fault
PKCF Proto-Kern Canyon fault
BF Breckenridge fault
WWF White Wolf fault
SNFF Sierra Nevada Frontal fault
FF Farewell fault
UNITS
Mesozoic granitic rocks
Paleozoic and Mesozoic pendant and wall rocks
ultramafic rocks
Franciscan assemblage
Rand and related schists
CA
Location of Figure
Mono Lake
Sierra Nevada Batholith
San Joaquin Valley
Salinian terrane
San Andreas Fault
Garlock Fault
Mojave Desert
Pacific Ocean
Southern California Batholith (SCB)
Peninsular Ranges Batholith
South Fork Valley
Area shown in Figure 2
(P)KCF
FF
KCF
PKCF
BF
WWF
SNFF
N
100 50 0 100
Km

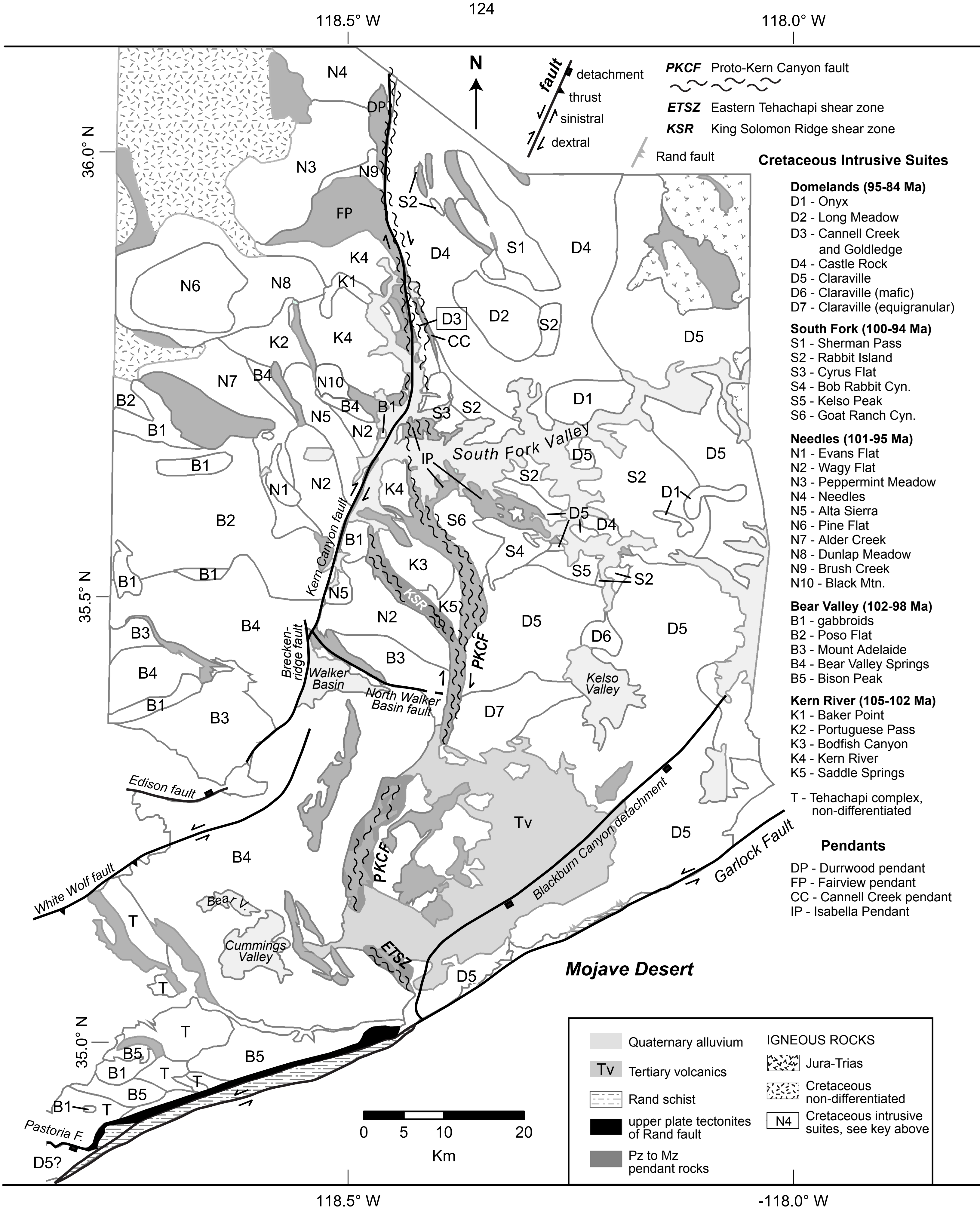

118.5° W
118.0° W
36.0° N
35.5° N
35.0° N
-118.0° W
N
fault
detachment
thrust
sinistral
dextral
Rand fault
PKCF Proto-Kern Canyon fault
ETSZ Eastern Tehachapi shear zone
KSR King Solomon Ridge shear zone
Cretaceous Intrusive Suites
Domelands (95-84 Ma)
D1 - Onyx
D2 - Long Meadow
D3 - Cannell Creek and Goldledge
D4 - Castle Rock
D5 - Claraville
D6 - Claraville (mafic)
D7 - Claraville (equigranular)
South Fork (100-94 Ma)
S1 - Sherman Pass
S2 - Rabbit Island
S3 - Cyrus Flat
S4 - Bob Rabbit Cyn.
S5 - Kelso Peak
S6 - Goat Ranch Cyn.
Needles (101-95 Ma)
N1 - Evans Flat
N2 - Wagy Flat
N3 - Peppermint Meadow
N4 - Needles
N5 - Alta Sierra
N6 - Pine Flat
N7 - Alder Creek
N8 - Dunlap Meadow
N9 - Brush Creek
N10 - Black Mtn.
Bear Valley (102-98 Ma)
B1 - gabbroids
B2 - Poso Flat
B3 - Mount Adelaide
B4 - Bear Valley Springs
B5 - Bison Peak
Kern River (105-102 Ma)
K1 - Baker Point
K2 - Portuguese Pass
K3 - Bodfish Canyon
K4 - Kern River
K5 - Saddle Springs
T - Tehachapi complex, non-differentiated
Pendants
DP - Durrwood pendant
FP - Fairview pendant
CC - Cannell Creek pendant
IP - Isabella Pendant
South Fork Valley
Kern Canyon fault
Breckenridge fault
Walker Basin
North Walker Basin fault
Kelso Valley
Edison fault
White Wolf fault
Bear V.
Cummings Valley
Blackburn Canyon detachment
Garlock Fault
Mojave Desert
Pastoria F.
D5?
Tv
0 5 10 20
Km
Quaternary alluvium
Tertiary volcanics
Rand schist
upper plate tectonites of Rand fault
Pz to Mz pendant rocks
IGNEOUS ROCKS
Jura-Trias
Cretaceous non-differentiated
N4 Cretaceous intrusive suites, see key above

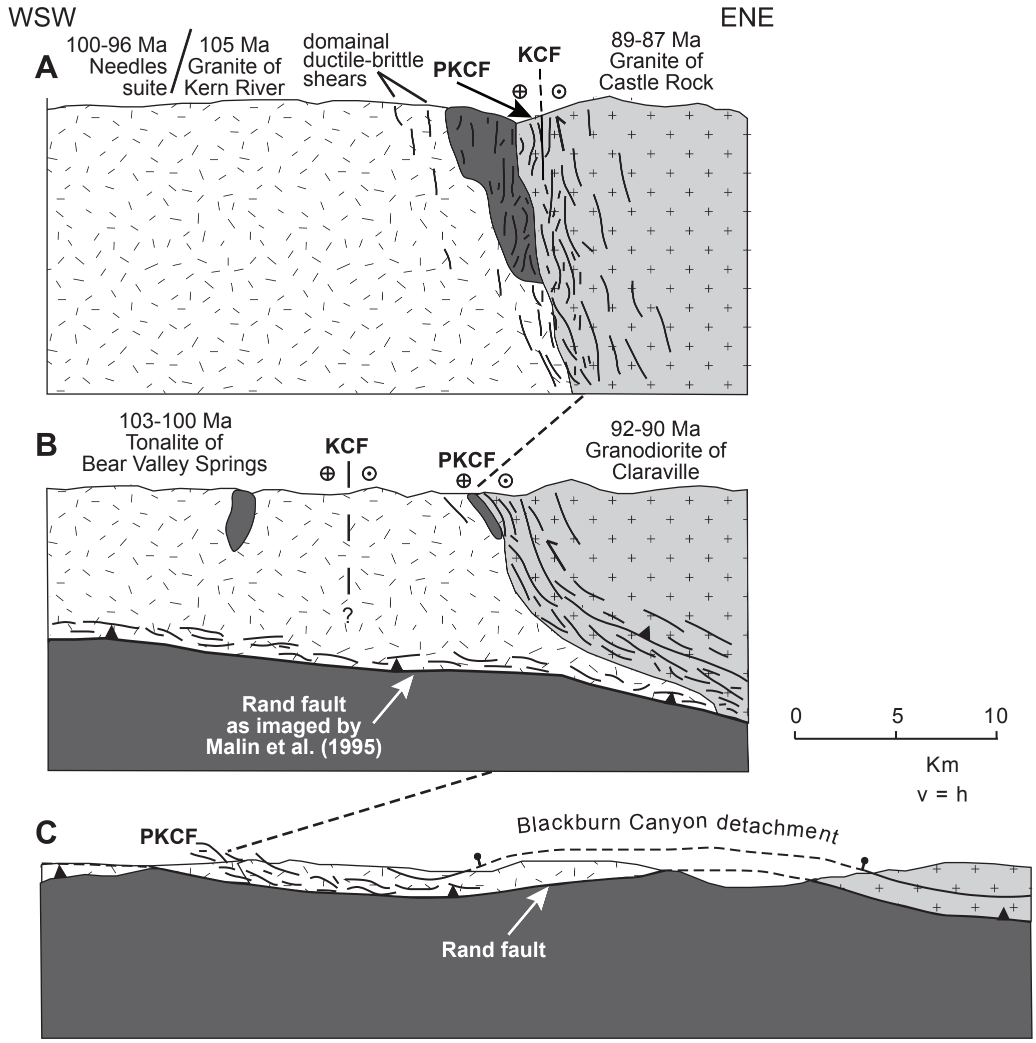
WSW
ENE
A
100-96 Ma
Needles
suite
105 Ma
Granite of
Kern River
domainal
ductile-brittle
shears
PKCF
KCF
89-87 Ma
Granite of
Castle Rock
B
103-100 Ma
Tonalite of
Bear Valley Springs
KCF
?
PKCF
92-90 Ma
Granodiorite of
Claraville
Rand fault
as imaged by
Malin et al. (1995)
0
5
10
Km
v = h
C
PKCF
Blackburn Canyon detachment
Rand fault

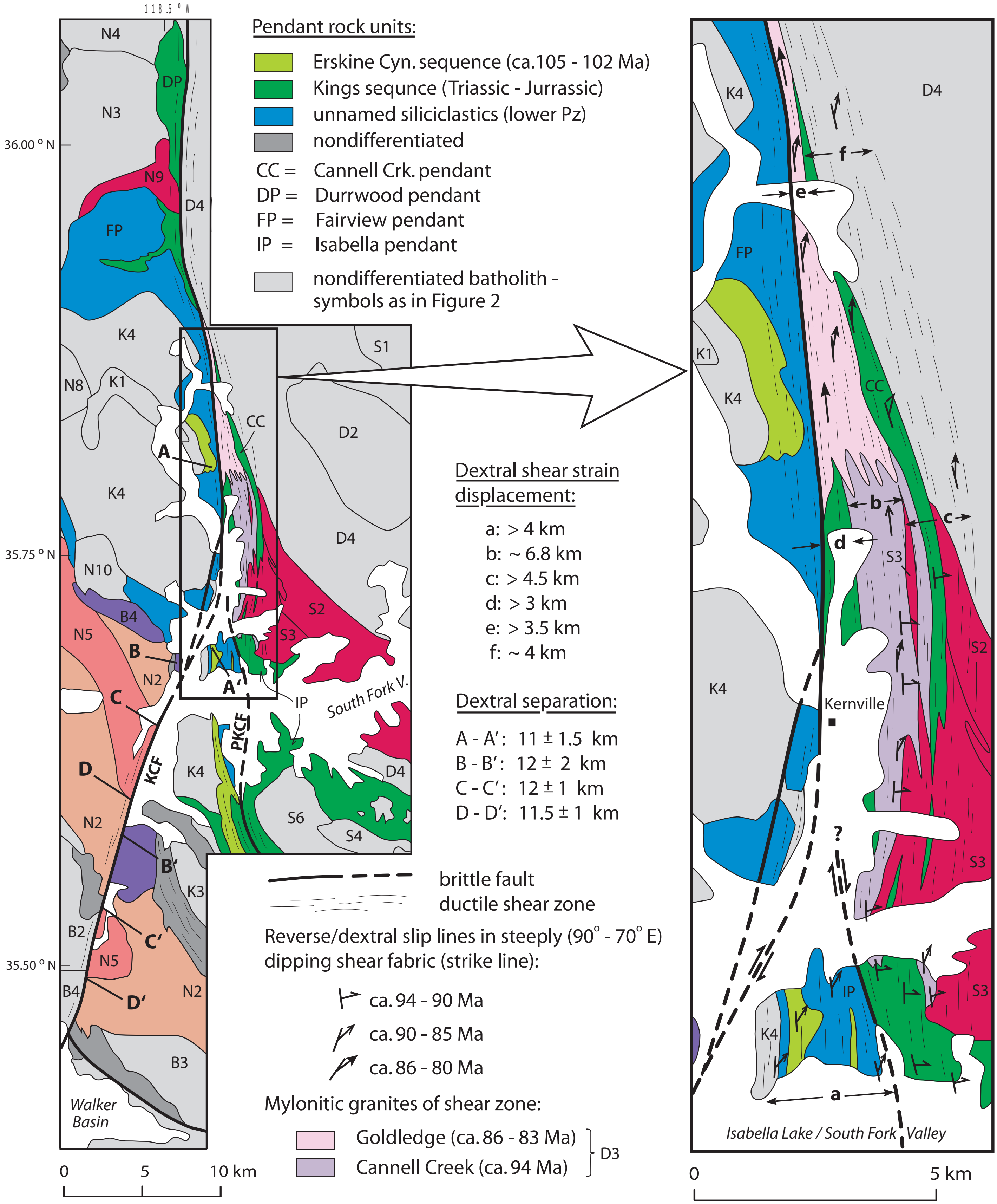

118.5° W
36.00° N
35.75° N
35.50° N
Pendant rock units:
Erskine Cyn. sequence (ca.105 - 102 Ma)
Kings sequnce (Triassic - Jurrassic)
unnamed siliciclastics (lower Pz)
nondifferentiated
CC = Cannell Crk. pendant
DP = Durrwood pendant
FP = Fairview pendant
IP = Isabella pendant
nondifferentiated batholith - symbols as in Figure 2
Dextral shear strain displacement:
a: > 4 km
b: ~ 6.8 km
c: > 4.5 km
d: > 3 km
e: > 3.5 km
f: ~ 4 km
Dextral separation:
A - A′: 11 ± 1.5 km
B - B′: 12 ± 2 km
C - C′: 12 ± 1 km
D - D′: 11.5 ± 1 km
brittle fault
ductile shear zone
Reverse/dextral slip lines in steeply (90° - 70° E) dipping shear fabric (strike line):
ca. 94 - 90 Ma
ca. 90 - 85 Ma
ca. 86 - 80 Ma
Mylonitic granites of shear zone:
Goldledge (ca. 86 - 83 Ma)
Cannell Creek (ca. 94 Ma)
D3
KCF
PKCF
South Fork V.
Walker Basin
Kernville
Isabella Lake / South Fork Valley
0 5 10 km
0 5 km

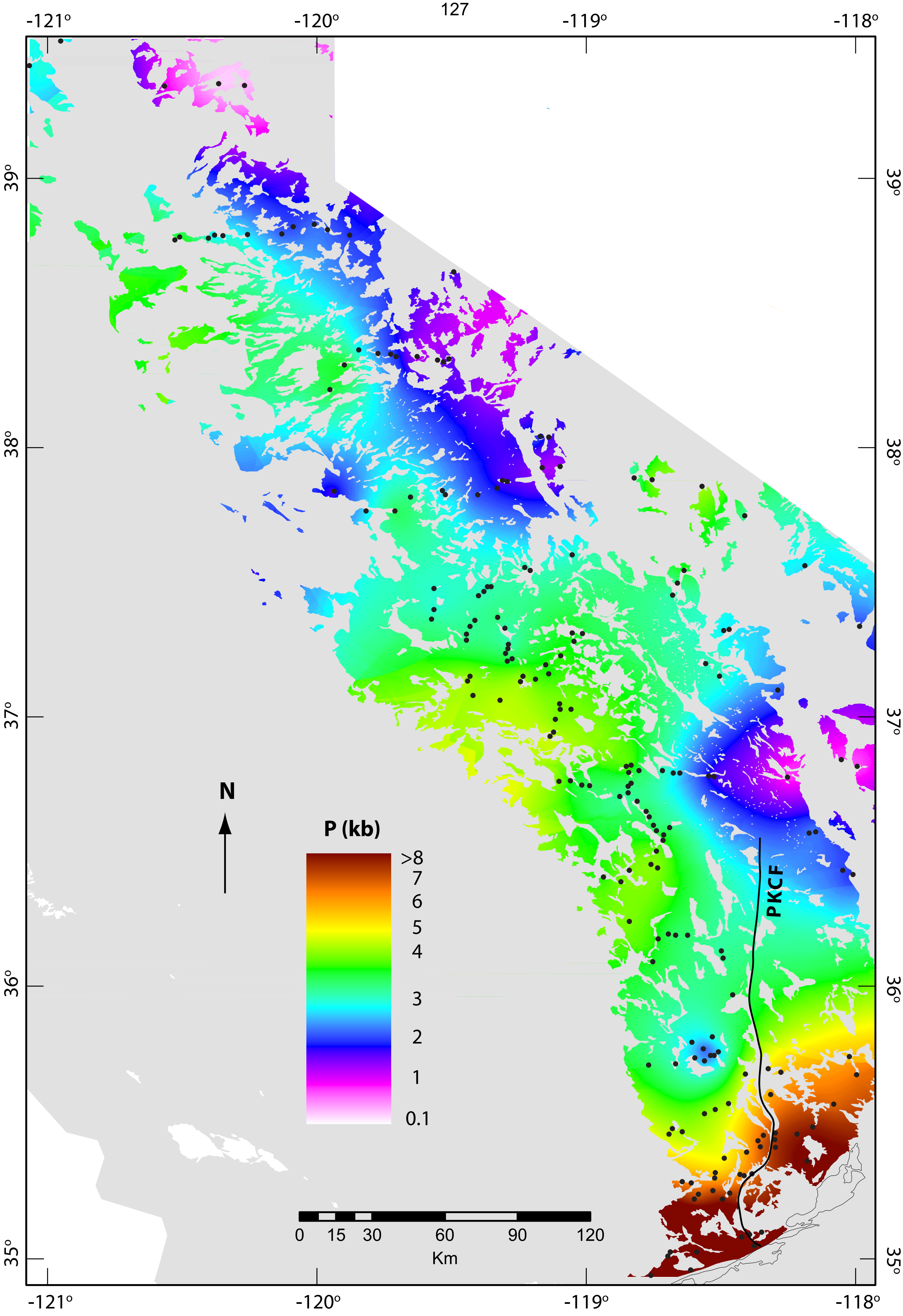

-121°
-120°
-119°
-118°
39°
38°
37°
36°
35°
N
P (kb)
>8
7
6
5
4
3
2
1
0.1
PKCF
0
15
30
60
90
120
Km

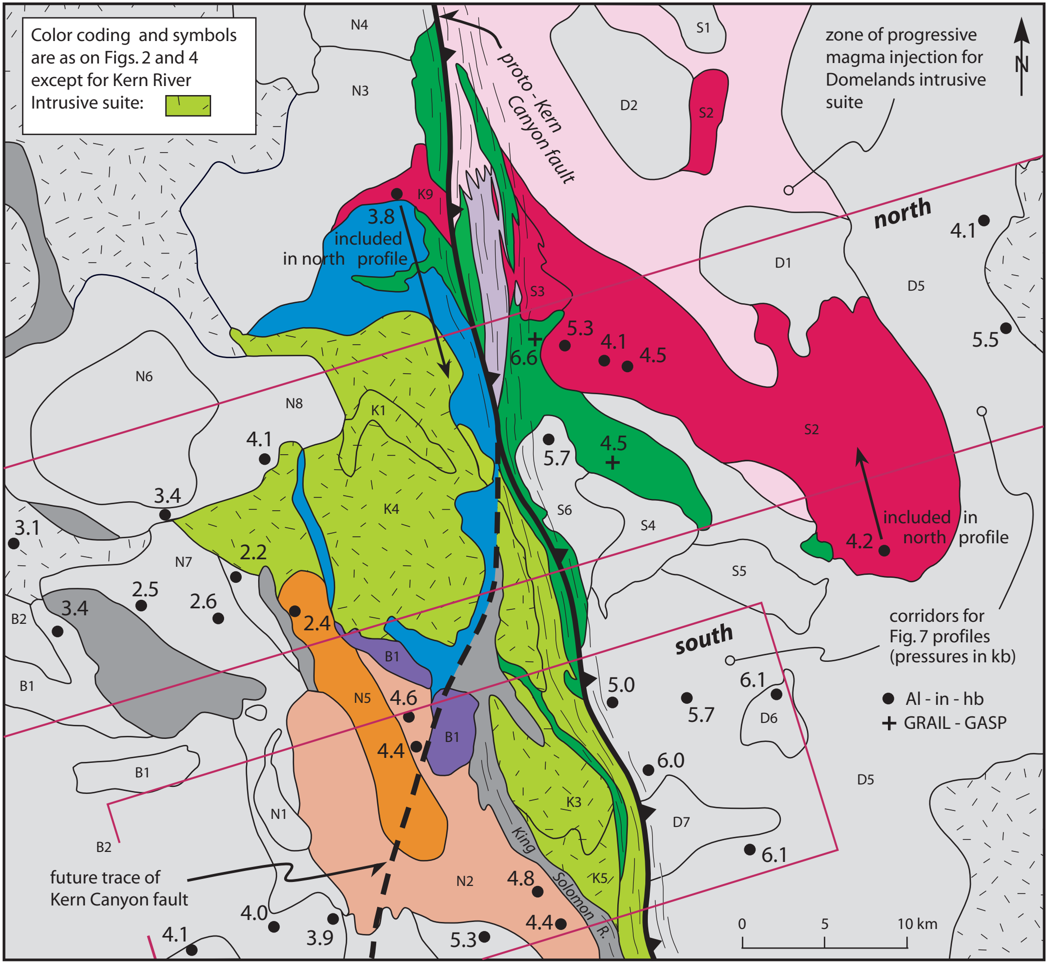
Color coding and symbols are as on Figs. 2 and 4 except for Kern River Intrusive suite:
proto - Kern Canyon fault
zone of progressive magma injection for Domelands intrusive suite
N
north
south
included in north profile
included in north profile
corridors for Fig. 7 profiles (pressures in kb)
Al - in - hb
GRAIL - GASP
future trace of Kern Canyon fault
King Solomon R.
0 5 10 km
N4
N3
N6
N8
N7
N5
N1
N2
S1
S2
S3
S4
S5
S6
D1
D2
D5
D6
D7
K1
K3
K4
K5
K9
B1
B2
3.8
5.3
4.1
4.5
6.6
4.5
5.7
4.1
5.5
4.2
4.1
3.4
3.1
2.2
2.5
2.6
3.4
2.4
4.6
4.4
5.0
5.7
6.1
6.0
6.1
4.8
4.4
4.0
3.9
4.1
5.3

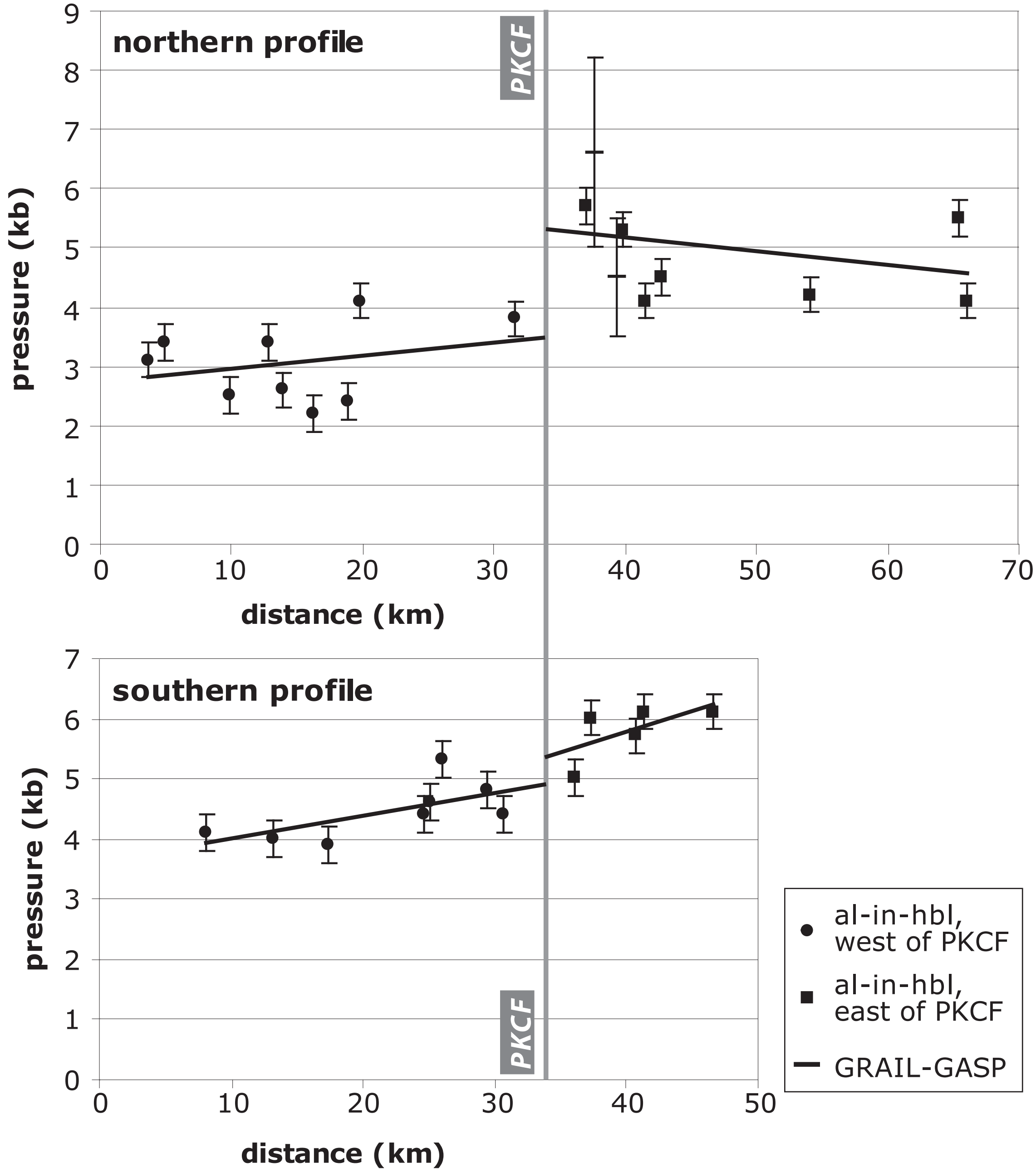
northern profile
PKCF
pressure (kb)
distance (km)
southern profile
PKCF
pressure (kb)
distance (km)
al-in-hbl, west of PKCF
al-in-hbl, east of PKCF
GRAIL-GASP

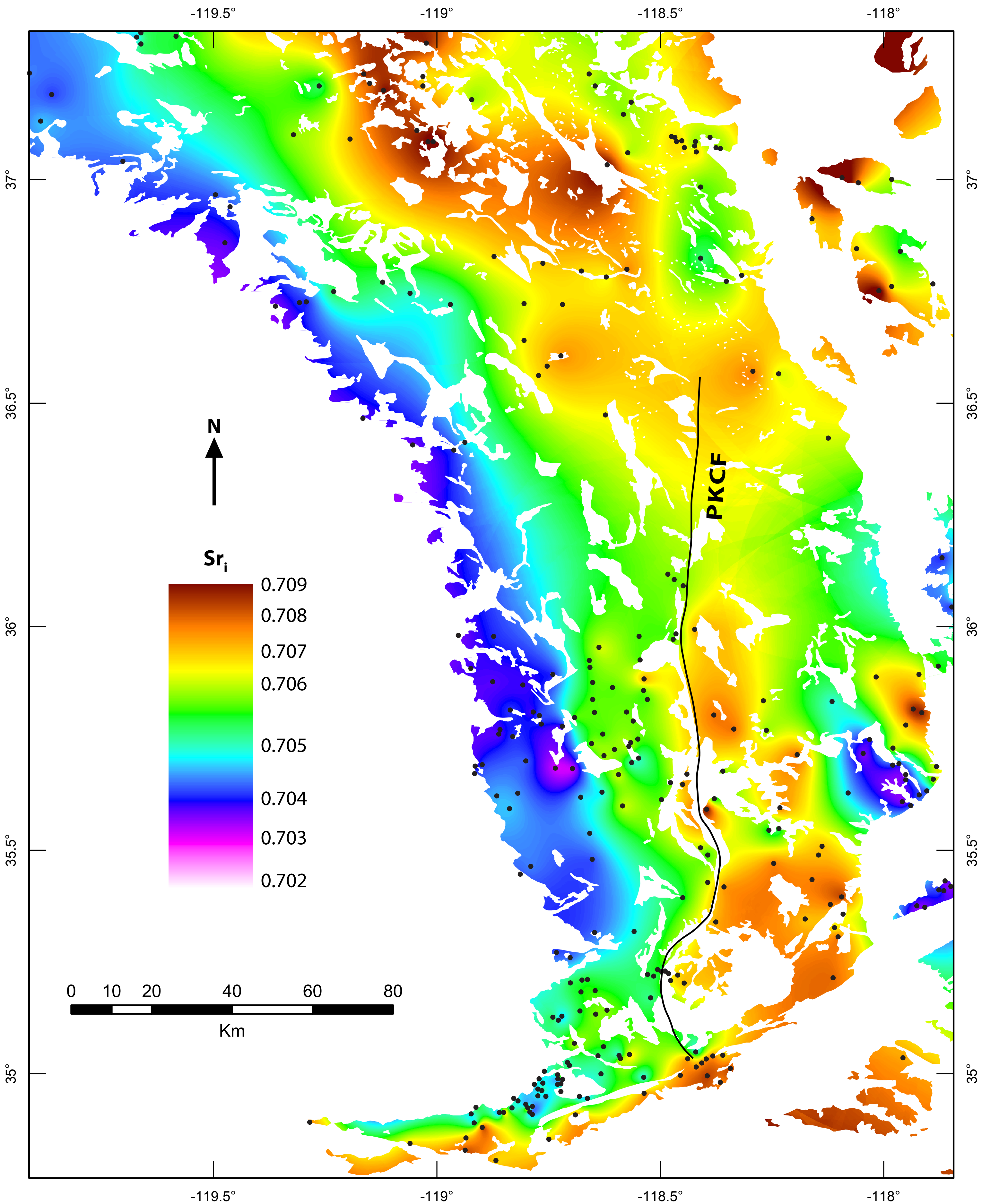
-119.5°
-119°
-118.5°
-118°
37°
36.5°
36°
35.5°
35°
N
PKCF
Sr$_i$
0.709
0.708
0.707
0.706
0.705
0.704
0.703
0.702
0 10 20 40 60 80
Km

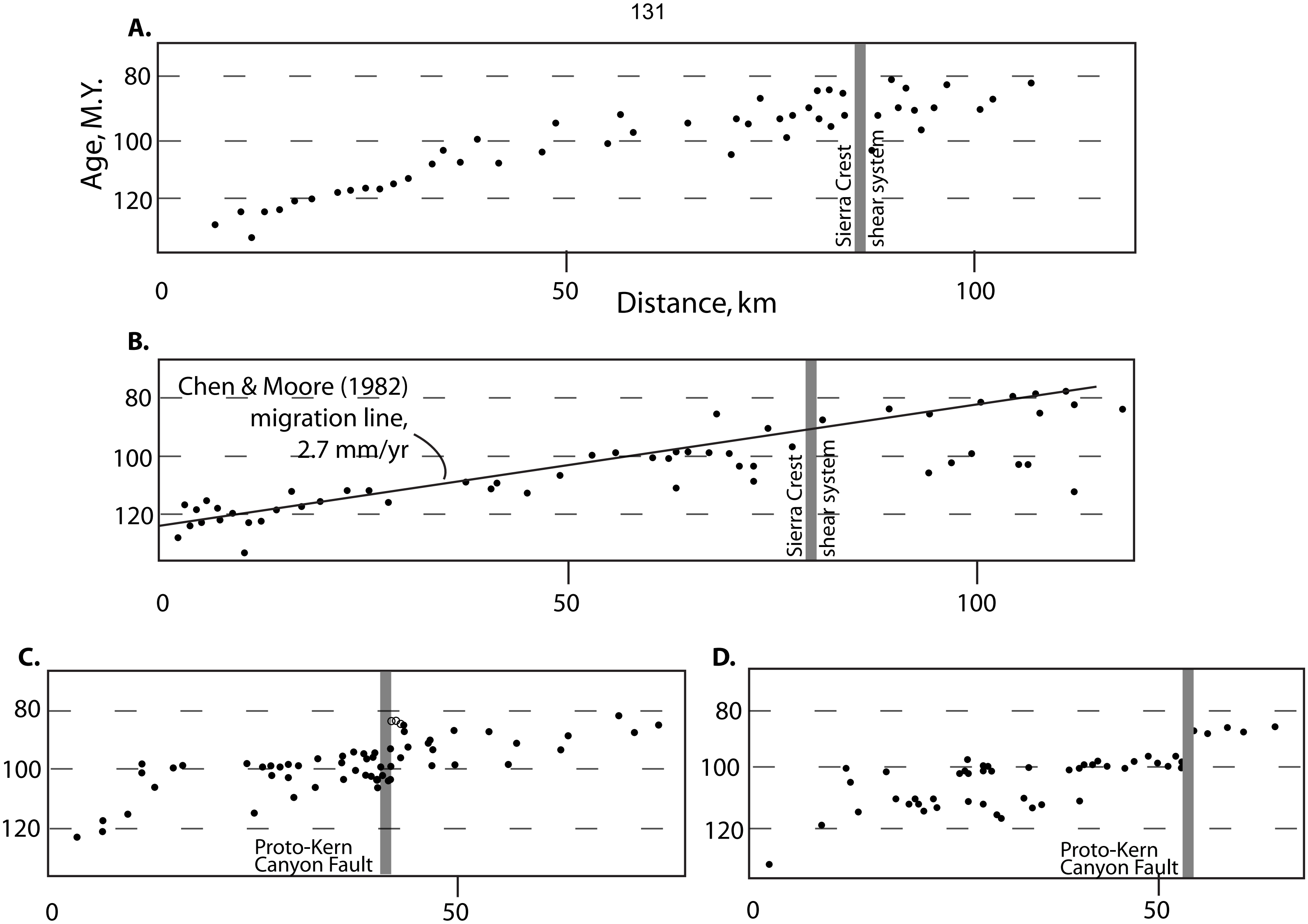
A.
Age, M.Y.
80
100
120
Sierra Crest shear system
0
50
100
Distance, km
B.
Chen & Moore (1982) migration line, 2.7 mm/yr
80
100
120
Sierra Crest shear system
0
50
100
C.
80
100
120
Proto-Kern Canyon Fault
0
50
D.
80
100
120
Proto-Kern Canyon Fault
0
50

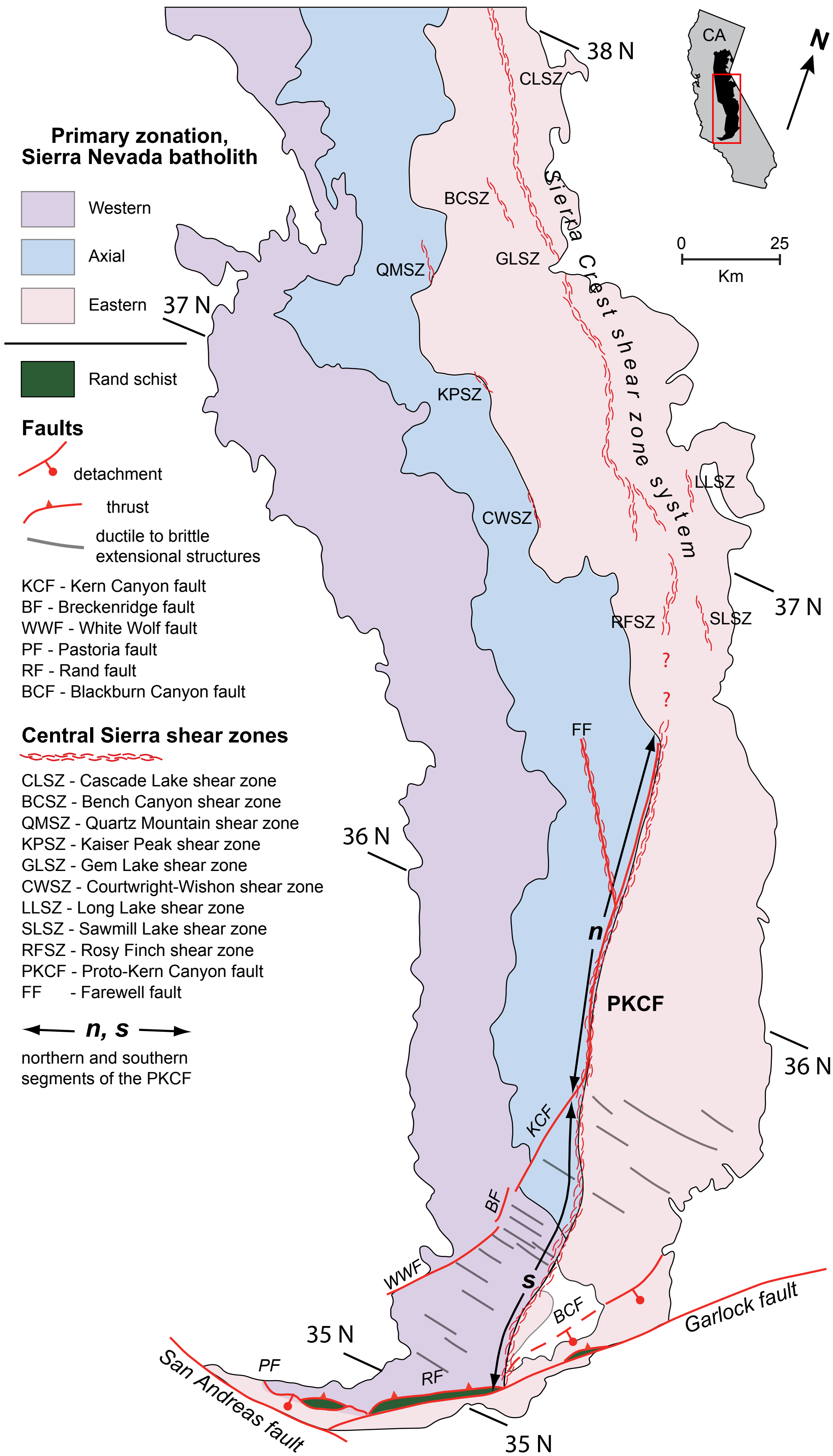
Primary zonation, Sierra Nevada batholith
Western
Axial
Eastern
Rand schist
Faults
detachment
thrust
ductile to brittle extensional structures
KCF - Kern Canyon fault
BF - Breckenridge fault
WWF - White Wolf fault
PF - Pastoria fault
RF - Rand fault
BCF - Blackburn Canyon fault
Central Sierra shear zones
CLSZ - Cascade Lake shear zone
BCSZ - Bench Canyon shear zone
QMSZ - Quartz Mountain shear zone
KPSZ - Kaiser Peak shear zone
GLSZ - Gem Lake shear zone
CWSZ - Courtwright-Wishon shear zone
LLSZ - Long Lake shear zone
SLSZ - Sawmill Lake shear zone
RFSZ - Rosy Finch shear zone
PKCF - Proto-Kern Canyon fault
FF - Farewell fault
n, s
northern and southern segments of the PKCF
38 N
37 N
36 N
35 N
CA
N
0
25
Km
Sierra Crest shear zone system
CLSZ
BCSZ
GLSZ
QMSZ
KPSZ
CWSZ
LLSZ
RFSZ
SLSZ
FF
n
PKCF
KCF
BF
WWF
s
BCF
Garlock fault
PF
RF
San Andreas fault

Cations	**02SS13**	**02SS16**	**03SS1**	**03SS5**	**03SS27**	**04SS27**	**04SS28**	**04SS31**
Si	6.74	6.77	6.78	6.69	7.34	6.82	6.65	6.62
Al iv	1.26	1.23	1.22	1.31	0.66	1.18	1.35	1.38
Al vi	0.29	0.26	0.24	0.27	0.21	0.21	0.25	0.14
Ti	0.12	0.14	0.13	0.15	0.06	0.14	0.13	0.15
Fe3+	0.28	0.36	0.44	0.41	0.08	0.42	0.45	0.56
Fe2+	1.93	1.73	1.93	2.11	1.90	1.71	1.86	1.62
Mn	0.06	0.06	0.08	0.07	0.06	0.05	0.06	0.07
Mg	2.31	2.45	2.19	1.98	2.67	2.47	2.25	2.46
Ca	1.92	1.92	1.89	1.88	1.85	1.91	1.94	1.90
Na	0.42	0.30	0.33	0.36	0.48	0.30	0.31	0.38
K	0.18	0.18	0.17	0.19	0.09	0.14	0.19	0.19
OH*	2.00	2.00	2.00	2.00	2.00	2.00	2.00	2.00
Sum	17.53	17.40	17.39	17.43	17.41	17.36	17.45	17.47
Al (t)	1.57	1.50	1.49	1.60	1.10	1.41	1.60	1.52
P (kb)	**4.47**	**4.13**	**4.09**	**4.60**	**2.20**	**3.68**	**4.59**	**4.22**

Cations	**04SS34**	**04SS37**	**04SS39**	**04SS42**	**04SS43**	**04SS44**	**04SS45**
Si	6.47	6.54	6.61	6.73	6.44	6.87	6.66
Al iv	1.53	1.46	1.39	1.27	1.56	1.13	1.34
Al vi	0.38	0.36	0.31	0.40	0.23	0.29	0.36
Ti	0.16	0.17	0.14	0.16	0.16	0.12	0.14
Fe3+	1.08	0.26	0.46	1.01	0.65	0.40	0.45
Fe2+	1.92	2.62	2.26	1.54	2.06	1.79	1.96
Mn	0.09	0.06	0.07	0.06	0.06	0.05	0.05
Mg	1.49	1.53	1.75	2.05	1.84	2.35	2.03
Ca	1.91	1.93	1.92	1.91	1.89	1.89	1.87
Na	0.40	0.37	0.38	0.36	0.35	0.28	0.31
K	0.28	0.27	0.24	0.21	0.22	0.14	0.19
OH*	2.00	2.00	2.00	2.00	2.00	2.00	2.00
Sum	17.70	17.57	17.53	17.69	17.47	17.31	17.37
Al (t)	1.91	1.82	1.68	1.68	1.79	1.42	1.70
P (kb)	**6.08**	**5.67**	**4.99**	**5.01**	**5.50**	**3.76**	**5.08**

Shear Zone (Fig. 10)	Kinematics	Timing	References
Proto-Kern Canyon Fault (PKCF)	East-side-up reverse thrust ductile shear Dextral ductile shear and faulting with minor reverse component Dextral brittle shear and faulting	ca. 95-90 Ma ca. 90-84 Ma ca. 84-79 Ma	Saleeby and Busby-Spera (1986, 1993), Busby-Spera and Saleeby (1990), Nadin (2007), Saleeby et al., (this volume), Saleeby and Nadin (in prep.)
Sawmill Lake (SLSZ)	East-side-up reverse ductile shear	ca. 95-90 Ma	Mahan et al., (2003)
Long Lake (LLSZ)	East-side-up reverse dextral ductile and brittle shear	ca. 94-90 Ma	Hathaway and Reed (1994)
Courtwright-Wishon (CWSZ)	East-side-up reverse ductile shear	ca. 102-86 Ma	Tobisch et al. (1995)
Kaiser Peak (KPSZ)	East-side-up reverse ductile shear	ca. 102-86 Ma	Tobisch et al. (1995)
Quartz Mountain (QMSZ)	East-side-up reverse ductile shear	ca. 102-86 Ma	Tobisch et al. (1995)
Bench Canyon (BCSZ)	East-side-up reverse ductile shear	ca. 102-86 Ma	Tobisch et al. (1995)
Rosy Finch (RFSZ)	Vertical lineations overprinted by horizontal thrusting followed by dextral shear	ca. 88-80 Ma	Tobisch et al. (1995), Tikoff and Saint Blanquat (1997), Tikoff and Greene (1994)
Gem Lake (GLSZ)	Vertical lineations overprinted by horizontal thrusting followed by dextral shear	ca. 88-80 Ma	Green and Dutro (1991), Sharp et al. (1993), Tikoff and Greene (1994), Greene and Schweickert (1995), Tobisch et al. (1995)
Cascade Lake (CLSZ)	Vertical lineations overprinted by horizontal thrusting followed by dextral shear	ca. 88-80 Ma	Davis (1996), Tikoff and Greene (1997)

North Profile

Pressure (kb)	Longitude	Latitude	Reference
3.1	-118.83	35.71	Ague & Brimhall, 1988
3.4	-118.73	35.71	Ague & Brimhall, 1988
2.5	-118.66	35.73	Ague & Brimhall, 1988
3.4	-118.67	35.80	Ague & Brimhall, 1988
2.6	-118.62	35.72	Ague & Brimhall, 1988
2.2	-118.59	35.75	Nadin
2.4	-118.78	35.74	Ague & Brimhall, 1988
4.1	-118.59	35.81	Ague & Brimhall, 1988
3.8	-118.52	35.97	Ague & Brimhall, 1988 **PKCF**
5.7	-118.38	35.60	Dixon, 1995
5.3	-118.33	35.67	Dixon, 1995
4.1	-118.34	35.68	Nadin
4.5	-118.33	35.67	Nadin
4.2	-118.14	35.56	Nadin
4.1	-118.08	35.74	Nadin
5.5	-118.06	35.67	Ague & Brimhall, 1988
6.6 (GASP-GRAIL)	-118.33	35.61	Dixon, 1995
4.5 (GASP-GRAIL)	-118.51	35.79	Dixon, 1995

South Profile

Pressure (kb)	Longitude	Latitude	Reference
4.1	-118.62	35.52	Ague & Brimhall, 1988
4.0	-118.58	35.54	Ague & Brimhall, 1988
3.9	-118.53	35.56	Ague & Brimhall, 1988
4.4	-118.47	35.67	Ague & Brimhall, 1988
4.6	-118.46	35.68	Nadin
5.3	-118.41	35.40	Ague & Brimhall, 1988
4.8	-118.41	35.43	Dixon, 1995
4.4	-118.38	35.44	Brady, 2004 **PKCF**
5.0	-118.36	35.45	Nadin
6.0	-118.38	35.44	Ague & Brimhall, 1988
6.1	-118.24	35.35	Ague & Brimhall, 1988
5.7	-118.28	35.46	Nadin
6.1	-118.22	35.48	Nadin